Noname manuscript No.
(will be inserted by the editor)

The Life Cycle of Active Region Magnetic Fields

M. C. M. Cheung
L. van Driel-Gesztelyi
V. Martínez Pillet
M. J. Thompson

Received: date / Accepted: date

Abstract We present a contemporary view of how solar active region magnetic fields are understood to be generated, transported and dispersed. Empirical trends of active region properties that guide model development are discussed. Physical principles considered important for active region evolution are introduced and advances in modeling are reviewed.

M. C. M. Cheung
Lockheed Martin Solar & Astrophysics Laboratory,
3251 Hanover Street, Palo Alto, CA 94304, USA.
and
National Astronomical Observatory of Japan,
2-21-1 Osawa, Mitaka, Tokyo 181-8588, Japan
E-mail: cheung@lmsal.com

L. van Driel-Gesztelyi
University College London, Mullard Space Science Laboratory
Holmbury St. Mary, Dorking, Surrey, RH5 6NT, U.K.
and
Konkoly Observatory, Research Centre for Astronomy and Earth Sciences,
Hungarian Academy of Sciences,
Budapest, Hungary
and
Observatoire de Paris, LESIA, CNRS, UPMC, Université Paris Diderot,
F-92195 Meudon Principal Cedex, France.
E-mail: Lidia.vanDriel@obspm.fr

V. Martínez Pillet
National Solar Observatory,
3665 Discovery Drive, Boulder, CO 80303, USA.
E-mail: vmpillet@nso.edu

M. J. Thompson
National Center for Atmospheric Research,
P.O. Box 3000, Boulder, CO 80307-3000, USA.
E-mail: mjt@ucar.edu

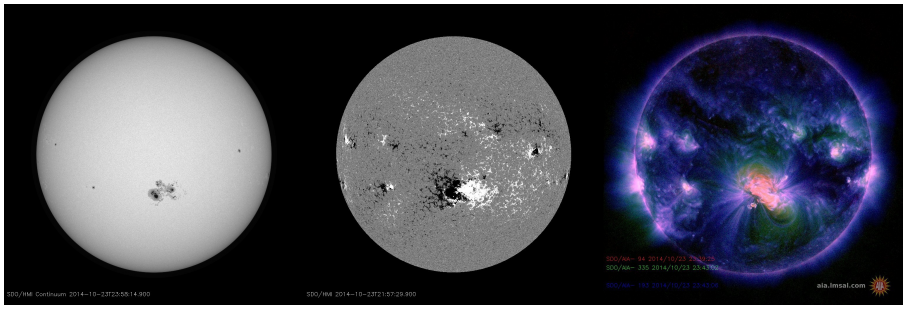

Fig. 1 Full-disk observations by NASA's Solar Dynamics Observatory (SDO) on 2014-10-23. The left and middle panels show a continuum image and line-of-sight magnetogram taken by the Helioseismic & Magnetic Imager (HMI), respectively. NOAA Active Region 12192, the largest sunspot group in cycle 24, appears as the dominant sunspot group and bipole in the southern hemisphere. The right panel shows a three-color composite EUV image (the 94, 335 and 193 Å channels of the Atmospheric Imaging Assembly (AIA) instrument) of the overlying corona.

1 Introduction

Magnetic activity on the Sun drives a diverse range of dynamic phenomena observed to occur on the solar surface and in the overlying atmosphere. The global-scale distribution of magnetic fields on the solar surface gradually evolves under the action of differential rotation, meridional circulation, and buffeting by supergranular flows. These processes operate steadily to mold and to erode the Sun's magnetic terrain.

Before high-precision and high-resolution spectropolarimetry became available, the solar surface was roughly delineated into active regions and quiet Sun regions. Active regions were associated with magnetic complexes in and around sunspots, while the quiet Sun was thought to be devoid of magnetic fields. With improved resolution and sensitivity, we now know the quiet Sun to be far from quiet. With Zeeman observations, we know the not-so-quiet Sun is filled with magnetic fields down to the smallest resolved scales ($\approx$ 100 km, e.g. Lites et al. 1996; Domínguez Cerdeña et al. 2003; Khomenko et al. 2003; Harvey et al. 2007; Lites et al. 2008; Ishikawa et al. 2008; Ishikawa & Tsuneta 2009; Danilovic et al. 2010b,a). With the Hanle effect and realistic convection modeling, turbulent fields have been inferred to exist at unresolved scales (Trujillo Bueno et al. 2004). Although the properties and origin(s) of ubiquitous quiet Sun magnetism is still under debate (see the review paper by Borrero et al. in this volume), comparative studies of quiet Sun field observations and radiative magnetoconvection simulations (e.g. Vögler & Schüssler 2007; Schüssler & Vögler 2008) suggest much of the quiet Sun magnetic field to be generated by a distributed small-scale dynamo operating throughout the bulk of the convection zone (Pietarila Graham et al. 2009; Danilovic et al. 2010b; Rempel 2014; Hotta et al. 2015, 2016).

What about the origin and life cycle of active region magnetic fields? The definition of what constitutes a solar active region has evolved as our un-

derstanding of solar magnetism has progressed in the last century. As suggested by van Driel-Gesztelyi & Green (2015), a useful modern definition due to Kiepenheuer (1968) is *'[the] totality of all observable phenomena preceding, accompanying and following the birth of sunspots'*. Figure 1 shows a subset of such observations from NASA's Solar Dynamics Observatory. Active regions leave their mark on the photosphere in the form of sunspot umbrae and penumbrae, pores, and surrounding areas of small-scale field. The intense magnetic fields threading sunspots penetrate the overlying atmosphere and structure the solar corona.

Sunspot magnetic fields have been extensively studied since their detection via the Zeeman effect in the early 20-th century (Hale 1908). How are magnetic fields on the Sun amplified, transported, and organized to form pores, sunspots and plages? How do the magnetic fields subsequently erode from sunspots, and where do they go? The life cycle of active regions is intimately connected to questions regarding the physical processes governing the global solar dynamo. The distribution of active region (old and new) magnetic fields on the solar surface shapes the global structure of the solar corona (Altschuler & Newkirk 1969; Schrijver & De Rosa 2003) and heliospheric current sheet (Riley et al. 2006), and determines the open flux of the interplanetary magnetic field (IMF; Wang et al. 2000; Lockwood et al. 2009; Jiang et al. 2011). Last but not least, non-potential (i.e. current-carrying) active regions spawn solar flares and coronal mass ejections (CMEs; Gosling 1993; Chen 2011; Webb & Howard 2012). So studying how active regions form, interact and decay is pertinent to our understanding of how the Sun's magnetism modulates space climate and space weather.

The physics of how the solar dynamo operates, how magnetoconvection modulates flux emergence, how active regions build up free energy to energize flares, and how they subsequently decay are all broad topics that deserve review papers in their own right. We do not aim for this paper to serve as a comprehensive reference for all topics associated with active regions. Rather, the aim is to synthesize the broad body of knowledge into a narrative summarizing our current understanding of the life cycle of active region magnetic fields. Our narrative begins with the subsurface origin of active regions.

2 The Subsurface Origin of Active Region Magnetic Fields

By all available observational accounts, sunspots form as large-scale flux bundles emerge from the solar interior onto the surface (see reviews by Zwaan 1978, 1985; Fan 2004, 2009; Lites 2009; Cheung & Isobe 2014; van Driel-Gesztelyi & Green 2015). At the scale of photospheric granulation ($L \sim 1$ Mm), the emerging flux reaches the surface as predominantly horizontal fields within the centers of granules (e.g. Cheung et al. 2007, 2008; Lites 2009; Ortiz et al. 2014). These are accompanied by opposite polarity patches anchored in the downflow lanes at the edges of granular cells. These telltale signs are evidence that granular-scale magnetic Ω-loops are transported to the surface from the

solar interior by convective flows (and perhaps aided by magnetic buoyancy, see section 5). Small-scale flux emergence events with these properties are not only found in developing active regions, but also in more quiet regions of the Sun (e.g. De Pontieu 2002; Centeno et al. 2007; Martínez González & Bellot Rubio 2009). In nascent active regions, ensembles of small-scale emergence events have a preferred orientation aligned with the final orientation connecting the leading and following polarity spots of the active region in a more mature state (Strous & Zwaan 1999; Pariat et al. 2004). Furthermore, opposite polarity patches stream in opposite horizontal directions. Like-polarity patches migrate in such a way that they coalesce into larger patches. When certain coherent patches have sufficient flux content ($\Phi \gtrsim 10^{19}$ Mx), pores (i.e. isolated umbral regions in the absence of penumbra) begin to appear. As the flux coalescence progresses, pores merge with adjacent pores and penumbral filaments begin to grow (e.g. Schlichenmaier et al. 2010). A detailed discussion of observations and theory concerning these 'phase transitions' is beyond the scope of this paper (we refer the reader to the review in this volume by Rempel & Scharmer, 2016). Rather, we emphasize that an apparent underlying driver rooted in the solar interior appears to move emerged flux patches in a systematic, non-random fashion.

Extensive theoretical and numerical investigations of coherent magnetic flux bundles rising through the convection zone have been carried out since Parker (1955) first pointed out how magnetic buoyancy drives their rise toward the surface (see the review by Fan 2009). Statistical properties of active regions, including Hale's law (Hale & Nicholson 1925) and Joy's law (Hale et al. 1919), provide observational tests for theories of the subsurface progenitors of active regions. Detailed studies of the surface evolution of individual active regions offer further clues regarding their subsurface structure.

As a example, Toriumi et al. (2014) carried out numerical magnetohydrodynamics simulations of the rise of buoyant flux tubes to mimic the observed photospheric evolution of sunspots in NOAA AR 11158. This active region appeared on the photosphere as two pairs of magnetic bipoles, and evolved such that the following polarity of one bipole jousted against the leading polarity of the other bipole, resulting in a sheared polarity inversion line which subsequently produced an X-class flare and CME. Toriumi et al. (2014) carried out simulations with initial conditions that consist of (i) two adjacent, submerged flux tubes each with a buoyant segment, and (ii) a single submerged tube with two magnetically buoyant segments. Both initial conditions yielded a pair of bipoles emerging at the surface, but only the latter case resulted in a sheared polarity inversion line amenable for eruptive activity. This result gives support to that view that the drivers of solar eruptive events lie beneath the solar surface.

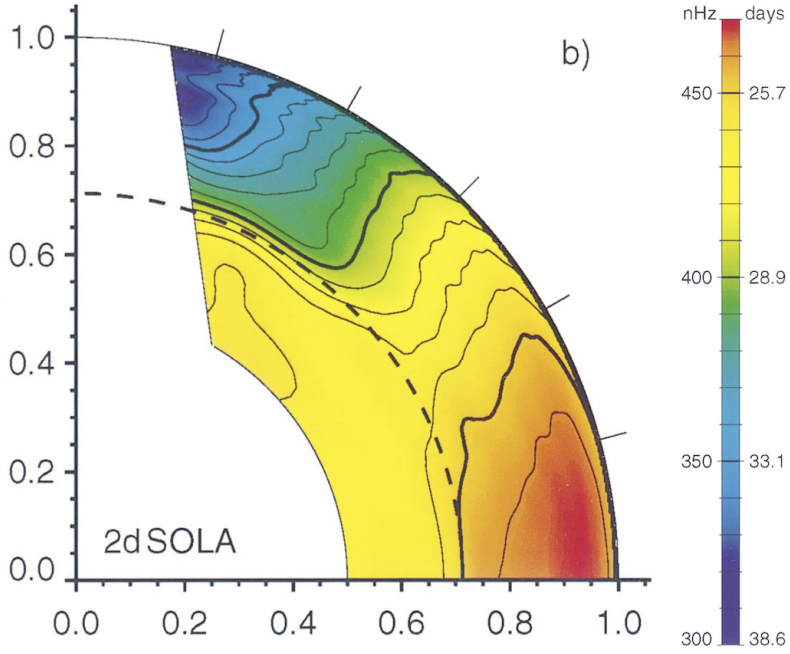

Fig. 2 Differential rotation profile of the solar interior from an inversion of global mode measurements by SoHO/MDI (figure adapted from Schou et al. 1998). The bottom of the convection zone is indicated by the dashed curve. Salient features include the conical rotation contours in the bulk of the convection zone, the solid body rotation in the radiative zone, the tachocline at low and high latitudes beneath the convection zone and the near-surface shear layer at low and mid-latitudes.

2.1 Helioseismic Constraints on Active Region Magnetic Fields

Helioseismology has taught us much about the properties of the solar interior, and offers the promise to teach us much about subsurface magnetic fields. So having adopted our working definition of active regions being the *'totality of observable phenomena preceding, accompanying and following the birth of sunspots'*, what observational constraints has helioseismology provided on the magnetic structure of active regions?

We first consider well-established helioseismology results that are relevant to, but not directly concerned with subsurface magnetic fields. Helioseismology has helped us learn about:

- The differential rotation profile $\Omega(r, \theta)$ throughout the bulk of the convection zone and in the upper radiative zone (Tomczyk et al. 1995; Thompson et al. 1996, 2003; Schou et al. 1998, see Fig. 2),
- The depth of the solar convection zone, indicated by the dashed line in Fig. 2 (Christensen-Dalsgaard et al. 1991),
- Patterns of meridional circulation (Giles 2000; Haber et al. 2002; Komm et al. 2013; Zhao et al. 2013), and

– Constraints on convective flows speeds (Hanasoge et al. 2012; Greer et al. 2015).

In the majority of global solar dynamo models, shearing by differential rotation, the so-called Ω-effect, plays a key role in the amplification of the mean azimuthal (toroidal) component of the magnetic field. In particular, certain mean-field (Krause & Rädler 1980) dynamo models require $\frac{\partial \Omega}{\partial r}$ to be positive or negative to give oscillatory solutions with equatorward propagating branches (mimicking the butterfly diagram, see Stix 1976). Helioseismic inversions of the rotation rate Ω as functions of radius and latitude have helped rule out the applicability of a number of such dynamo models.

The quasi-solid body rotation in the radiative core was an unexpected discovery (Thompson et al. 1996, 2003). This hints at the possible existence of a fossil field contained within the radiative core whose Maxwell stresses keep the core rotating as a solid body (MacGregor & Charbonneau 1999). However, such a fossil field would presumably not undergo polarity reversals between cycles and so likely is not the birthplace of active region magnetic fields.

The tachocline, which is the region of transition from solid body rotation to radial isorotation profiles was recognized to contain large shear and so is a candidate for the operation of the Ω-effect (which, in some models, leads to strong toroidal fields that become buoyant unstable and rise toward the surface). The tachocline is prolate and at low latitudes lies substantially beneath the base of the convection zone. The region where rotational shear and convectively stable stratification coexist is thought to provide a suitable region for toroidal magnetic field to be generated and stored until it becomes buoyant and rises towards the surface.

According to flux-transport models, meridional circulation plays a key role in the working of the dynamo and in setting the length of the solar cycle. In such models the meridional flow advects flux from decaying active regions to the poles and causes the reversal of the poloidal component of the solar magnetic field in the polar regions. The simplest models envisaged a single cell in depth spanning from surface down to the deep convection zone. Time-distance helioseismic analysis of about 2 years of ground-based Global Oscillation Network Group (GONG) data by Jackiewicz et al. (2015) and 4 years of SDO/HMI data by Rajaguru & Antia (2015) support the existence of such a single meridional cell filling the entire convective zone. These studies dispute the reported detection of multiple cells structure in depth (Zhao et al. 2013) and in latitude (Schad et al. 2013; Zhao et al. 2013). The implications of multiple meridional cells for flux-transport dynamos have been explored by Hazra et al. (2014) and Belucz et al. (2015).

3 Active regions and ephemeral regions

The magnetic pattern on the solar surface is continuously seeded by the emergence of magnetic loops over a range of spatial and temporal scales (Schrijver et al. 1997; Parnell 2001; Simon et al. 2001; Hagenaar et al. 2003; Meyer

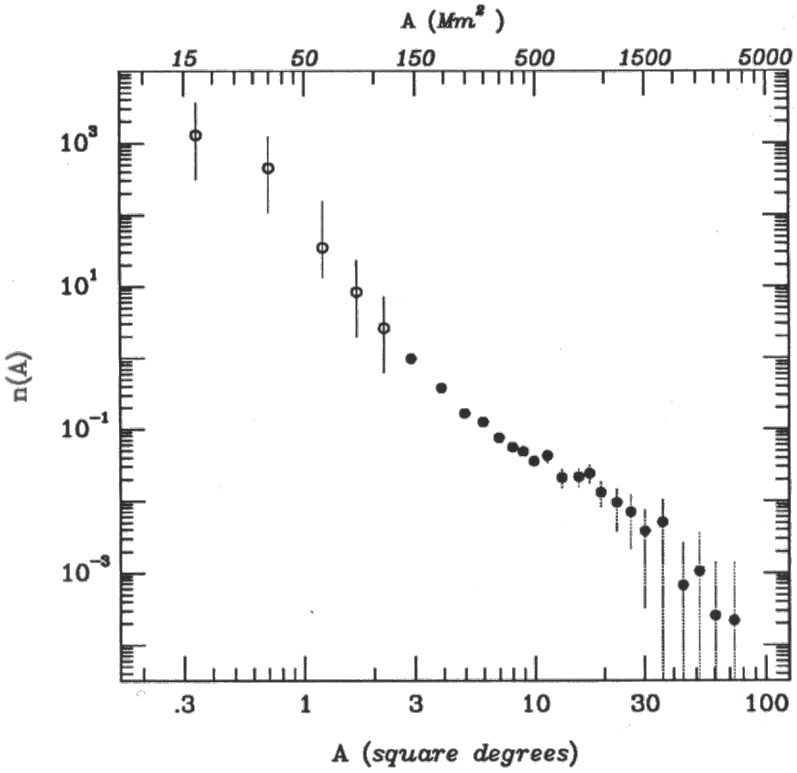

Fig. 3 Size distribution of 978 active regions (solid dots) and 9492 ephemeral regions (open dots) identified from Kitt Peak full-disk magnetograms (reproduced from Figure 17, Chapter 8 of Harvey 1993). The measured quantity $n(A)$ corresponds to the number of bipolar regions with surface area A at the time of maximum development. For members in the sample with area $A > 3.5$ square degrees, the power-law shape of the size distribution was found to persist throughout Cycle 21 though the absolute appearance rates differed by a factor of 8 between cycle minimum and maximum.

et al. 2011; Iida et al. 2012; Gošić et al. 2014). To study where, when and how these loops appear is to get a glimpse of how the subsurface reservoir of dynamo-generated magnetic field feeds the surface. Some properties of the largest magnetic bipoles, the active regions are well-known. As a statistical ensemble, they yield Hale's Polarity Rule, Joy's Law and the butterfly diagram. What about their smaller counterparts? Are they simply smaller versions of the same phenomenon? Do they share a common origin? In summary, are ephemeral regions active regions?

This is one of the important questions addressed by K. L. Harvey in her PhD thesis. Harvey (1993) used daily Kitt Peak full-disk magnetograms taken throughout the duration of Cycle 21 (between 1975 through 1986) to examine the statistical properties of bipolar active regions and ephemeral regions (see also Harvey & Zwaan 1993). Figure 3 shows the size distribution histogram of magnetic bipoles corresponding to 978 active regions (solid dots) and 9492

ephemeral regions (open dots) identified over the entire data set. Their sample of bipolar regions included only ones that emerged and reached their maximum development on the visible hemisphere (although they correct for this observational limitation). The size distribution $n(A)$ for the entire sample, defined as the number of regions with area A per square degree per day, was found to follow a power-law. For active regions with $A \gtrsim 3.5$ square degrees, the absolute emergence rate varied in phase with the solar cycle with a modulation amplitude of 8 though the shape of the distribution remained unchanged. For smaller active regions with $2.5 \lesssim A \lesssim 3.5$ square degrees, the modulation amplitude is about 5. For ephemeral regions with $A \lesssim 2.5$ square degrees, the modulation amplitude is further diminished to a value of 2.

The emergence frequency is not the only property of magnetic bipoles that depends on the area. The distribution of orientation (tilt angles) of magnetic bipoles was also found to be size-dependent. Bipoles with $A \gtrsim 2.5$ square degrees had orientation distributions that are mostly consistent with Hale's polarity rule and Joy's law. However the bias in the preferred orientation diminishes with decreasing A and is virtually non-existent for $A \lesssim 2.5$ square degrees. Furthermore, the distribution of emergence latitudes follow the equatorward propagating branches of the butterfly diagram but the latitudinal spread of the distributions widen with decreasing A. Based on these findings, Harvey (1993) conclude that ephemeral regions are the smaller-scale manifestation of active regions over a continuous spectrum of magnetic bipolar regions spanning almost three orders of magnitude in size.

The seminal work by Harvey (1993) was extended by Hagenaar et al. (2003), who used full disk magnetogram data from the Michelson Doppler Imager (MDI) on board the Solar and Heliospheric Observatory (SoHO) to study the size distribution of ephemeral bipolar regions. Their study differs from Harvey (1993) in some important ways. Whereas Harvey (1993) manually tracked bipolar active regions, Hagenaar et al. (2003) used a fully automated algorithm. The algorithm (detailed in Hagenaar 2001) implements the following two steps. The first step involves the segmentation of individual magnetograms into discrete magnetic features with each magnetic feature consisting of contiguous pixels of like magnetic polarity (above some sensitivity threshold). The second step is the matching up of magnetic features in consecutive magnetograms (96 minute cadence) satisfying certain spatiotemporal criteria. This automated method only detects newly emerged regions and does not track the development of detected bipolar regions to maximum development and beyond. In lieu of active region area, the Hagenaar et al. (2003) study measures the size distribution in terms of magnetic flux content. Since the algorithm is designed to only detect new bipolar emergences that occur within 96 minute intervals, the detected emergence events are restricted to ephemeral regions (and small bipolar regions) with fluxes in the range $\Phi = 3 \times 10^{18} - 4 \times 10^{20}$ Mx. The lower end of the range of fluxes is limited by the sensitivity of MDI magnetograms and the thresholding criteria used for feature detection. The upper end of the range presumably corresponds to an upper limit to the flux emergence rate of ephemeral regions and of small and large active regions in

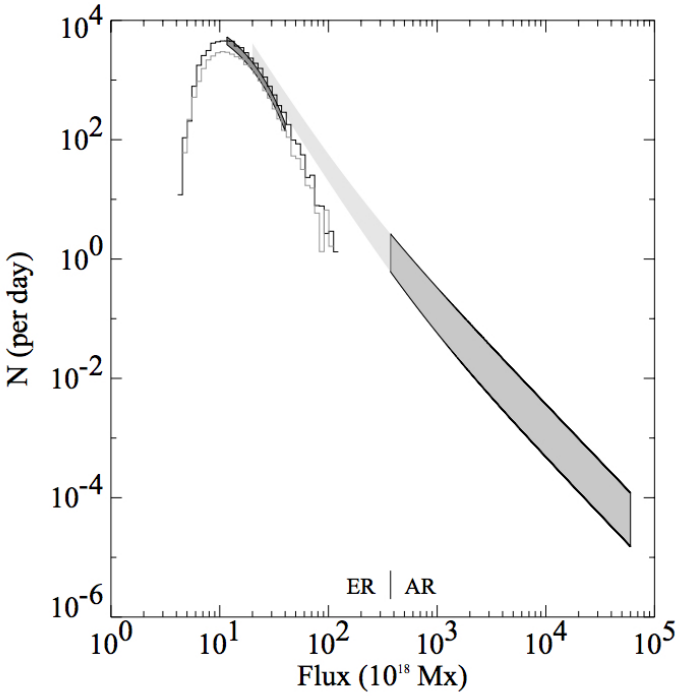

Fig. 4 Appearance rate of bipolar regions as a function of magnetic flux (reproduced from Fig. 11 of Hagenaar et al. 2003). The curves in the range $\Phi \lesssim 10^{20}$ Mx indicate distributions of ephemeral regions identified in SoHO/MDI magnetograms. The black and gray curves indicate distribution functions for data sets taken in Oct 1997 and Aug 2000, respectively. The drop off in emergence rates at the leftmost end of the flux range is attributed to limits in the detection sensitivity of the algorithm for the available data sets. The range of emergence rates reported by Harvey (1993) covering solar minimum to maximum (in cycle 21) is indicated by the diagonal light and dark gray bands in the right half of the plot. The light gray band indicates emergence rates for the ephemeral regions and active regions identified in that study.

their infancy. Hagenaar et al. (2003) fitted decaying exponential profiles (with Φ as the independent variable) to bipolar emergence frequencies at different times between 1996 (minimum between Cycles 22 and 23) and 2001 (one year past the maximum of Cycle 23). They report a variation of the bipolar appearance rate in *antiphase* with the sunspot cycle with a modulation amplitude of at most 1.5.

Based on the results of Harvey (1993, see also Harvey & Zwaan, 1993) and their own study of ephemeral regions, Hagenaar et al. (2003) produced the composite distribution of bipolar regions shown in Fig. 4. The magnetic bipole areas measured by Harvey (1993) were converted to magnetic flux content assuming a given area-to-flux ratio. The drop off in emergence rates at $\Phi < 10^{19}$ Mx is attributed to the sensitivity of the detection algorithm and source

of data (MDI magnetograms). Disregarding that turn off, the bipole emergence rate is seen to be a smoothly decreasing function over four orders of magnitude in magnetic flux Φ.

From the size, tilt and orientation distributions from the Kitt Peak data set, Harvey (1993) concluded *'ephemeral regions are in the extrapolation of the small-scale end of a wide size spectrum of bipolar magnetic regions'*. At first glance, the findings by Hagenaar et al. (2003) would suggest a similar conclusion. However, Hagenaar et al. (2003) arrive at a markedly different interpretation. They propose that Harvey's findings and their own are *'compatible with an interpretation in which there are two distinct, but coupled origins of solar bipolar regions: (1) a globally operating cyclic dynamo and (2) a near-surface, small-scale dynamo'*.

It is perhaps timely to assess whether the remarkable suggestion offered by Hagenaar et al. (2003) holds up against more recent developments. As already mentioned in the introduction, there is now substantial empirical evidence that the solar surface is pervaded by mixed turbulent fields down to the smallest observable scales. Hinode spectropolarimetric observations of the Fe I 6302.5 Å photospheric line taken in quiet Sun regions near disk center show no significant variations of the turbulent field signal over the time period spanning 2006 to 2012 (Buehler et al. 2013).

The terms 'local dynamo' and 'surface dynamo' are often used (sometimes interchangeably) in the literature as labels for the physical system responsible for generating the cycle-independent portion of the observed magnetic field. These terms carry the connotation that there is a clear segregation between the global cyclic dynamo and the mechanism generating small-scale magnetic flux. As numerical experiments of convective dynamos may suggest, segregation may well be an oversimplification. For instance, Rempel (2014) used the radiative MHD code MURaM to carry out a number of small-scale dynamo experiments in a Cartesian domain. The convective flows in the model are driven by radiative cooling at the surface as computed by solving the radiative transfer equation with realistic opacities and equation of state (the net vertical energy flux carried by convective motions below the surface and by radiation above corresponds to one solar luminosity). The Cartesian domain has a bottom boundary located at a few Mm below the surface and is open to inflows and outflows. Rempel (2014) examined the dependence of the surface magnetic flux densities on the choice of the bottom boundary condition. In the case where magnetic flux is prevented from entering the domain through upflows crossing the bottom boundary, the convective dynamo still operates but maintains unsigned flux at a level below what is reported from observations (~ 85 G). One possible resolution to this incompatibility with observed values of the unsigned flux is to allow inflows from the bottom boundary to advect magnetic flux into the domain. Rempel (2014) tested this scenario by enforcing that the r.m.s. field strength $B_{\rm rms}$(as a function of depth) scale with the equipartition field strength ($B_{\rm eq} = (4\pi\varrho)^{1/2} v_{\rm rms}$) corresponding to the r.m.s. speed $v_{\rm rms}$ of convective flows. This setup led to surface field strengths in agreement with observations. If this case were representative of the solar

interior, it would implicate feeding of flux from the deeper layers to the shallower layers as an important contributor to the surface magnetic flux budget. It would suggest that the convective dynamo operates over the bulk of the convection zone and is not localized near the solar surface (Fan & Fang 2014; Hotta et al. 2015, 2016).

4 The small- and large-scale dynamos as a coupled system

In light of the aforementioned observational and theoretical developments, perhaps we should reframe the scientific discourse on the 'two dynamos' and the origin of active regions versus the origin of small-scale bipoles. If one takes the view that turbulent convection drives a distributed dynamo that operates over the bulk of the solar convection zone, one may expect magnetic fields to be generated and maintained over a continuous range of scales. At small scales (e.g. smaller than supergranulation) where the convective overturning times are short and the associated Rossby number ($Ro = \frac{P_{\rm rot}}{\tau_{\rm conv}}$, where $P_{\rm rot}$ and $\tau_{\rm conv}$ are the rotation period and convective turnover time, respectively) is large, rotational effects such as the Coriolis force are small. In this regime, the dynamo-generated magnetic field patterns (at these scales) are expected to follow distribution functions with essentially random tilt angles and be largely insensitive to the phase of the solar cycle. This expectation is consistent with the properties of the smallest ephemeral regions. At larger scales (where $Ro < 1$), rotational effects such as shear and helical motions become important. Firstly, large-scale differential rotation is important for the generation of mean-field toroidal flux (Babcock 1961). Secondly, rotational motions generate helical magnetic fields, which in a turbulent medium exhibit an inverse cascade of magnetic helicity. This means the storage of magnetic twist migrates from the small scales to the large scales (Brandenburg 2001).

To summarize, both observations and theory indicate the lack of a clear separation of scales between the small and the large, between the convection-dominated and the rotation-dominated regimes. So perhaps we should ask the following questions: In a turbulent stellar interior like the Sun's convection zone where both the large and the small co-exist, what are the physical processes that govern the formation of magnetic bundles that become active regions? How does intermittency (i.e. the formation and destruction of spatially and temporally coherent structures) and order (i.e. systematic behavior followed by active regions) emerge (pun intended) out of this chaotic system? Do the small-scales impact the efficiency of magnetic flux generation at large (global) scales? The recognition that the global cyclic behavior of active regions and the details of magnetoconvection are intimately linked is pushing the limits of our understanding of the solar dynamo, and with that our understanding of the life cycle of active region magnetic fields. Recent advances have been enabled by numerical models of convective dynamos, a topic we will discuss in the following section.

5 The Cradle of Active Region Magnetic Fields

Parker (1955) first proposed the idea that sunspots form following the buoyant rise of magnetic flux tubes from the solar interior onto the surface. The underlying MHD concept is simple. Suppose a magnetic bundle is in pressure equilibrium with its surroundings. Due to the contribution of magnetic pressure $B^2/8\pi$ to the total pressure inside the tube, the interior gas pressure is reduced relative to the external gas pressure. Further assume the plasma in the interior and exterior are in thermal equilibrium. This requires a density deficit within the tube of order $\frac{\Delta\varrho}{\varrho} \sim -\frac{1}{\beta}$, where β is the ratio of gas to magnetic pressures (in the deep convection zone $\beta \gg 1$). Due to this density deficit, a flux tube has buoyancy and will rise toward the surface.

Parker assumed the existence of toroidal bands of magnetic field in the solar interior whose polarities switch from one sunspot cycle to the next. Such expectations motivate the search for certain mean-field dynamo models (Krause & Rädler 1980; Rädler 1980) with cyclic, wave-like solutions. While mean field dynamo (e.g. see Stix 1976; Moffatt 1978) solutions describe how the toroidal and poloidal components of the azimuthally-averaged field evolve, they do not provide a self-consistent picture for how active regions (and the associated Ω-type magnetic bundles) form. Nevertheless, the existence of a mean component of the toroidal field led researchers to study the linear (in)stability of thin magnetic flux tubes (Spruit & van Ballegooijen 1982; van Ballegooijen 1982; Ferriz-Mas & Schüssler 1993, 1995) subject to azimuthal perturbations.

The non-linear evolution of flux tube instabilities was studied by means of numerical simulations solving MHD equations that describe how coherent, slender flux tubes evolve under the influence of magnetic buoyancy, aerodynamic drag and the Lorentz and Coriolis forces (Spruit 1981; Choudhuri 1990; Longcope & Klapper 1997) in a rotating reference frame. A detailed review of developments within the so-called *thin flux tube approximation* is outside the scope of this paper. For that we refer the reader to Fan (2009). For our purpose we merely summarize some important results. First of all, the Coriolis force $(2\varrho\mathbf{\Omega} \times \mathbf{v})$ is found to deflect flux tubes rising from the bottom of the convection zone. This happens in two steps. First of all, the Coriolis force drives a retrograde flow in a rising flux tube (to conserve angular momentum). This motion then induces the Coriolis force to impart momentum to the flux tube in a direction parallel to the axis of rotation. Flux tubes with initial $B \lesssim 10^5$ G are deflected to latitudes higher than emergence latitudes of observed active regions on the Sun (Choudhuri & Gilman 1987; Choudhuri 1989). Since the sunspot cycle is approximately 11 years and sunspots groups appear over a large fraction of the cycle, the growth times of buoyancy instabilities are expected to be in the range of hundreds of days. For much shorter growth times, the underlying toroidal field would be prematurely depleted. For much longer growth times, buoyancy instabilities would not lead to the creation of sunspot groups. Schüssler et al. (1994) reported a threshold of $B \sim 10^5$ G to satisfy this requirement. For flux tubes initially located at latitudes within ± 70 deg of the equator in the overshoot layer, the $m = 1$ and $m = 2$ modes

(m being the azimuthal number of the perturbation) have the highest growth rates. Furthermore, for flux tubes at these field strengths (and with flux content $\Phi \sim 10^{22}$ Mx), the thin flux tube model yields results that are consistent with empirically reported relationships between active region tilt and emergence latitude (see also D'Silva & Choudhuri 1993; Caligari et al. 1995), tilt and magnetic flux content (Fan et al. 1994; Fisher et al. 1995) and the scatter of active region tilt about Joy's law (Longcope & Fisher 1996).

Thin flux tube calculations have been used to study the development of asymmetries between the leading and following flanks of rising Ω-loops. Asymmetries can be characterized by a number of properties, such as the difference in the vertical orientation and the difference in field strengths between the two flanks. Caligari et al. (1998) compared model results from two types of initial conditions, those in (1) initial mechanical equilibrium ("MEQ", e.g. Moreno-Insertis et al. 1994; Caligari et al. 1995) in the overshoot layer, and those (2) with initial undulations and in thermal balance ("TBL", e.g. Fan et al. 1993) with the ambient stratification such that the crests are initially buoyant and already located in the convection zone. For initial field strengths of $B \sim 10^5$ G, the two types of initial conditions yield opposite results. For instance, MEQ (TBL) flux tubes have following flanks that are more (less) vertical than their leading counterparts. Caligari et al. (1998) consider the MEQ results to be more compatible with the observed proper motions of young active regions. The results from the two types of initial conditions are similar for tubes with weaker field ($B \sim 3 \times 10^4$ G). At these lower field strengths, both MEQ and TBL flux tubes approach the solar surface with the following flank more vertical and possessing stronger field strengths. In section 5.1, we will discuss how flux tubes with 3×10^4 G initial strength are perhaps more consistent with observations when the interaction of the tube with convective flows is taken into account.

It is unclear the asymmetries in thin flux tube models are physically compatible with observational reports of relatively longer lifetimes of leading spots compared to following spots. For example, Meyer et al. (1977) assumed the following leg of an Ω-loop to be more inclined to the radial direction (opposite to the results of dynamical thin flux tube calculations) and invoked the interchange instability to explain the relatively shorter lifetimes of following spots. Rempel & Cheung (2014) perform a numerical MHD simulation of active region formation by emerging a magnetic loop with an imposed flow mimicking the retrograde flow driven by the Coriolis force. They found the leading polarity model spot to remain coherent longer than the following polarity spot. However, their simulations only capture the top 15 Mm of the convection zone and do not self-consistently treat the Coriolis effect. Further detailed investigations are necessary to clarify which physical effect may be responsible for morphological asymmetries in active regions.

Longcope & Klapper (1997) extended the thin tube model to treat flux tubes with magnetic twist. In their model, magnetic field lines within the tube are not assumed to be aligned within the tube axis. In addition to other quantities like field strength, mass density and momentum, the extended model

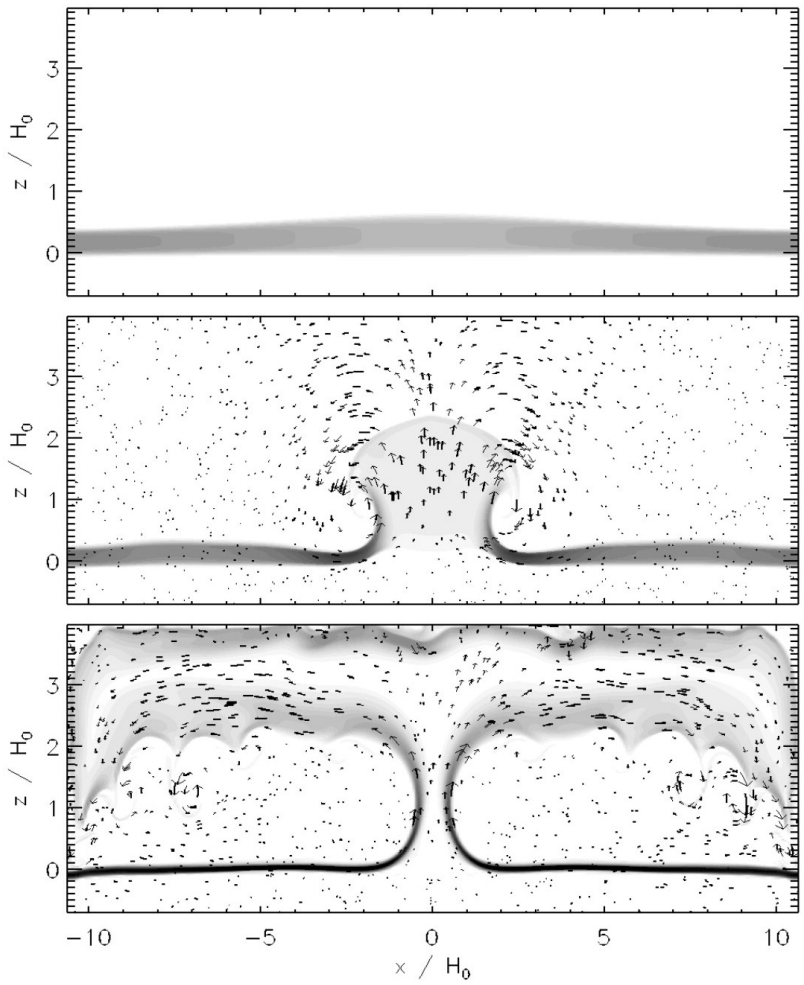

Fig. 5 Idealized 2D MHD simulation of the subsurface 'explosion' of an Ω-loop (from Rempel & Schüssler 2001). Following the explosion, the magnetic field in the horizontal portions of the loop is intensified.

solves for the magnetic pitch $q(l)$ as a function of position along the tube axis. Magnetic pitch is defined by the relation $B_\phi(l) = q(l) r B_l(l)$, where B_l and B_ϕ are, respectively, the longitudinal and transverse components of the magnetic field and r is the radial distance from the tube axis. By solving for $q(l)$, the Longcope & Klapper (1997) model captures important dynamical effects relevant to active region evolution. These include (1) the origin of active region twist (Longcope et al. 1998), (2) the relation between active region writhe and twist (Longcope et al. 1998), and (3) the driving mechanism for sunspot rotation (by magnetic torque) and injection of free energy into the corona (Longcope & Welsch 2000).

The apparent success of the thin flux tube models to reproduce well-known statistical properties of active regions on the Sun (and on other cool stars, see Schüssler et al. 1996; Granzer et al. 2000) opens up further questions about the origin of active region magnetic fields. For instance, how can flows near the bottom of the convection zone amplify magnetic fields to 100 kG? Depending on the model of the convection zone (e.g. 1D mixing length model or 3D dynamic model), the magnetic energy density associated with such fields is estimated to be $10 - 100$ times the kinetic energy density of typical convective flows in the lower half of the convection zone. So Lorentz force feedback would likely prevent the amplification of magnetic fields to such strengths by convective flows (or, for that matter, the shear at the tachocline). One possible mechanism for intensification of magnetic fields to super-equipartition strengths was suggested by Moreno-Insertis et al. (1995). Working within the thin flux tube framework, they reported how Ω-loops from initial flux rings with $B = 10^4$ G fail to emerge because they experience dramatic expansion and weakening before reaching the surface. In the thin flux tube model, such a subsurface 'explosion' leads to a pressure gradient within the Ω-loop which sucks material out of the legs of the tube toward loop apex. Rempel & Schüssler (2001) modeled this process using 2D MHD simulations (see also Rempel 2001; Hotta et al. 2012, for corresponding models in 3D). As illustrated in Fig. 5, the rise of an Ω-loop through a super-adiabatically stratified layer (mimicking the convection zone) can lead to an abrupt expansion of the loop apex (even before it reaches the surface). The resulting pressure gradients drive upflows through the legs of the loop, which partially evacuates the anchored portions of the tube. The partial evacuation of the anchored portions leads to pressure deficit and subsequent compression. The combined action of the vertical compression and the stretching by outflows leads to an intensification of the magnetic field. Rempel & Schüssler (2001) suggest the repeated occurrence of such explosions may produce the superequipartition fields that are required by thin flux tube models for reproducing active region properties.

5.1 Magnetic Flux Tubes in a Convective Environment

Even as one grapples with the question of how 10^5 G fields may be generated inside the convection zone, one may also question whether such strong fields are really necessary, or just a requirement of overly simplified models. In particular, the thin flux tube models referenced above assume that the flux tubes do not interact with convective flows. They also assume that a solitary tube remains coherent on its journey through the turbulent convection zone. Does the picture change when convective turbulence is considered? The extent to which magnetoconvective effects are included varies widely between models. We first discuss models with the simplest treatment of convective turbulence before proceeding to review state-of-the-art models of 3D convective dynamos in Sun-like stars.

The consideration of the effects of convective turbulence on the life history of active region magnetic fields introduces both conceptual and technical challenges. When convective eddies interact with a rising flux tube, do they leave the flux tube intact or whitewash its identity either by enforcing magnetic reconnection at the scale of the eddies, or by turbulent diffusion? How does momentum transfer between a flux tube and convective eddies affect the former's trajectory (if it remains coherent)? A quantitative examination of the various effects relies on helioseismic measurements (or constraints) on the power spectrum of convective flows within the convection zone, which is a challenging technical feat in itself (e.g. compare results from Hanasoge et al. 2012; Greer et al. 2015).

The action of the Coriolis force on sufficiently large and long-lived flow structures results in net helical motion, which is characterized by a systematic correlation between horizontally diverging flows (associated with convective upflows) and vertical vorticity of one sign, and horizontally converging flows with vertical vorticity of the opposite sign (e.g. see Hathaway 1982; Rüdiger et al. 1999; Gizon & Duvall 2003). The importance of the Coriolis effect can be estimated by the Rossby number $Ro = (2\tau_c \mathbf{\Omega} \cdot \hat{g})^{-1}$, where τ_c is the lifetime (or correlation time) of turbulence, $\mathbf{\Omega}$ is the rotational velocity and $\hat{g}$ the unit vector for gravitational acceleration. For $Ro \lesssim 1$, the turbulent flows are rotationally constrained. Based on this simple analysis, surface granulation flows are too short lived to be rotationally constrained. However, larger scale, longer lived flows are expected to be modified by rotational effects. The action of the Coriolis is expected to generate clockwise motion in diverging flows in the northern hemisphere and anti-clockwise motion in the southern hemisphere. This expectation is supported by flow maps of the top few Mm of the convection zone from time-distance helioseismology inversions (Langfellner et al. 2015, see Fig. 6) and from surface flow maps derived from correlation tracking of photospheric magnetic patterns (Hathaway et al. 2013). As we shall see below, the helical nature of turbulence in the solar convection zone has important implications for the generation of twist in magnetic flux tubes.

The effect of angular momentum exchange between buoyant magnetic tubes and convective eddies was first considered by Choudhuri & D'Silva (1990) for axisymmetric thin flux tubes. They considered two scenarios. The first involves so-called 'giant cells', which the authors treat as a uniform, radially directed upflow that exert upward drag on rising tubes. In effect, this means a rising tube is no longer experiencing drag relative to a stationary background, but against a background with a net outflow velocity. For a range of field strengths, they found that an outflow with an amplitude of tens of m s^{-1} or more is sufficient to move flux tubes radially to $R = 0.9R_\odot$. At shallower depths, the flux tube expands so much that buoyancy and aerodynamic drag are negligible compared to the Coriolis force, which deflects tubes to latitudes beyond the Sun's activity belts.

In the second scenario, Choudhuri & D'Silva (1990) considered how interaction of the flux tube with small-scale turbulence can erode the tube's angular momentum. This effect is captured by adding a drag term to the azimuthal

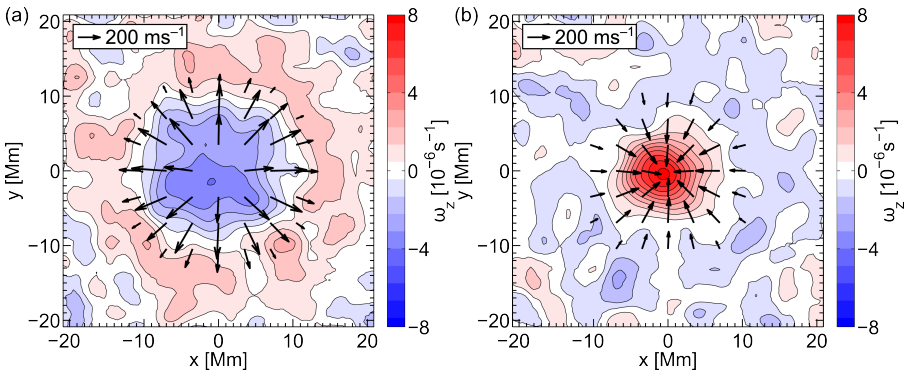

Fig. 6 Time-distance (TD) helioseismology flow maps averaged (a) divergent and (b) convergent regions (reproduced from Langfellner et al. 2015). These flow maps were computed by averaging over several thousand supergranules at a latitude of +40 deg and are representative of flows at depths between zero and a few Mm. The color-scale in both panels indicate the sign and magnitude of the average vertical component of flow vorticity (ω_z). This work shows that, at the supergranule-scale, diverging (converging) flows are correlated with negative(positive) vorticity in the northern hemisphere.

component of tube's equation of motion. For an initially stationary flux tube in a rotating frame, the tube gains angular momentum in a retrograde sense due to the Coriolis force. This in turn leads to a Coriolis force which deflects the tube poleward. Choudhuri & D'Silva (1990) suggested that the interaction between the flux tube and turbulent convection can reduce the angular momentum of the tube, which in turn may lead the flux tube (even those with initial field strengths of 10 kG, i.e. equipartition) to emerge within the Sun's activity belts. It should be noted that the effect of differential rotation in the solar interior is not considered in this early work. Instead, the effective drag of the background convection on the tube is computed assuming the background has zero angular velocity in the rotating reference frame. As can be seen in Fig. 2, except for the near-surface shear layer, $\frac{\partial \Omega}{\partial r} > 0$ within the bulk of the convection zone at latitudes below 30 deg. So the interaction between a rising flux tube and the super-rotating medium may be have a more pronounced effect than was reported by Choudhuri & D'Silva (1990).

Turbulent convective flows are expected to influence more than just the emergence latitude of rising magnetic tubes. The scatter of measured active region tilt angles far exceeds their latitudinal averages, being particularly large during the early emerge phase of active regions. Longcope & Fisher (1996) attribute the large scatter in tilt angles to stochastic interactions of convective flows with a rising flux tube. Using a mixing length model for the convection zone, they performed Monte Carlo simulations of thin flux tubes rising buoyantly while being buffeted by convective flows. The randomly generated convective flows modify the aerodynamic drag experienced by different sections of the tube and in doing so introduce scatter in the tilts of emerging Ω loops. When the initial field strength of the tube is 30 kG, the amplitude of the scatter in tilt angle generated by the Monte Carlo models compares well

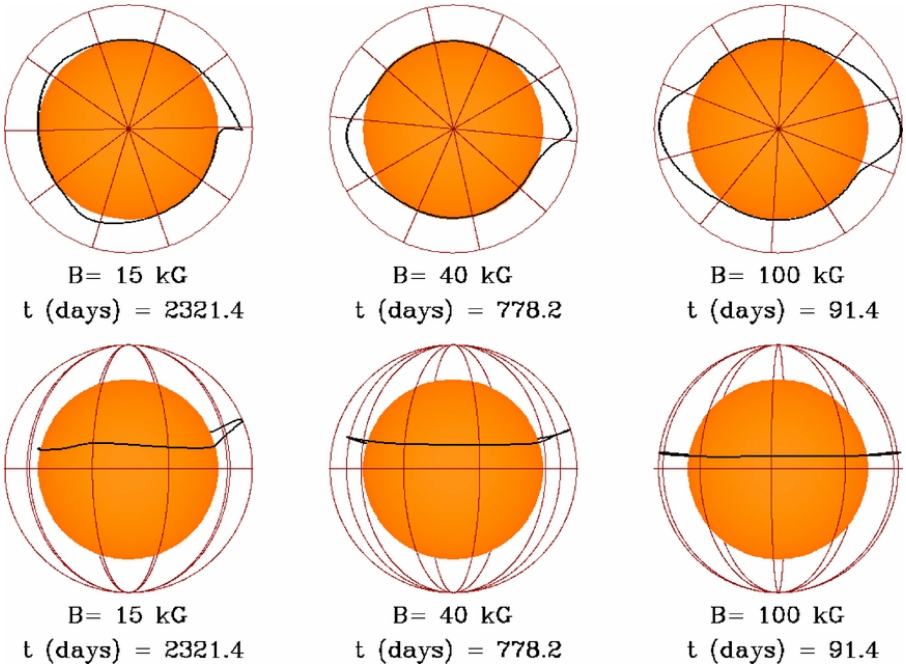

Fig. 7 Shapes of toroidal flux tubes (with initial strengths from $B = 15$ to $B = 100$ kG) at the time when the apices of the tubes reach the top boundary ($r = 0.97R_\odot$). This figure is reproduced from Weber et al. (2011) and shows flux tubes evolving in the absence of convective flows.

against observational results. Furthermore, ensemble averages reproduce the latitudinal dependence of the tilt angles.

The most sophisticated of thin flux tube models were carried out by Weber et al. (2011, 2013). Instead of parameterizing the effect of turbulent convective flows, they computed the aerodynamic drag force on the tube by using the 3D flow structure from a hydrodynamic global convection simulation. This non-magnetic convection model was tuned (in terms of latitudinal entropy gradient and the bottom and top boundaries and radial profiles of viscous and thermal diffusivities) to give solar-like differential rotation (see Fig. 2). Figures 7 and 8, respectively, show the shapes of the magnetic tubes (with flux $\Phi = 10^{22}$ Mx) at a time when their apices reach the top boundary ($r = 0.97R_\odot$) of the simulation domain in the absence and presence of convective flows. In the absence of convection, the rise time of a flux tube with an initial field strength of $B = 15$ kG takes about half a sunspot cycle. Even a tube with initial $B = 40$ kG takes a couple of years to reach the top boundary. In contrast, the rise times of flux tubes in a convective environment is on the order of months irrespective of the initial field strength. In the Weber et al. (2013) study, they carried out a large parameter study by varying magnetic fluxes from $\Phi = 10^{20}$ to 10^{22} Mx, field strengths from 15 to 100 kG and by sampling different realizations of the convective flow pattern. They conclude that flux

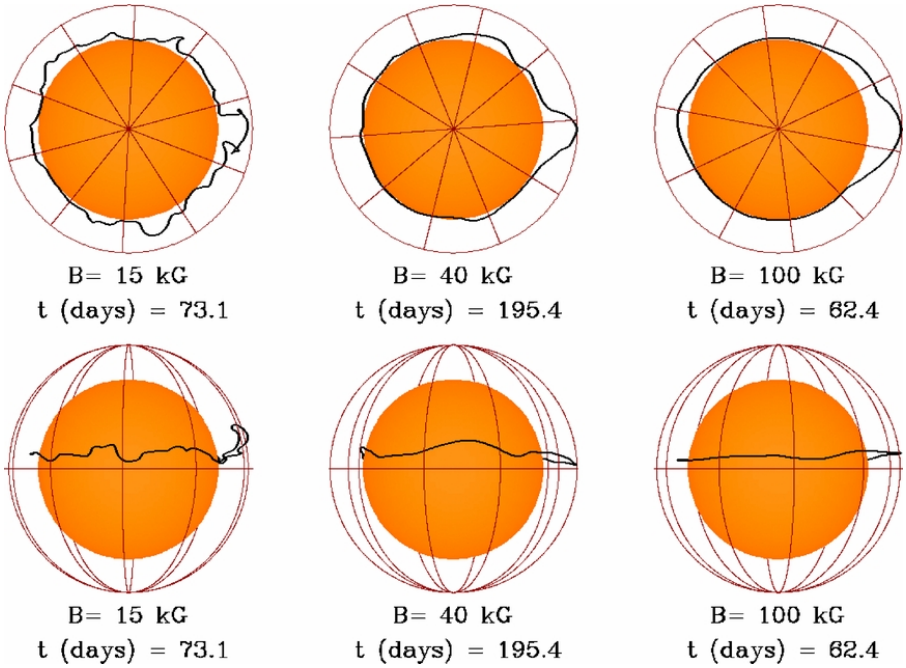

Fig. 8 Same as Fig. 7 but for flux tubes evolving against a 3D convection model.

tubes with initial field strengths of $B \gtrsim 40$ kG produce active region properties that are most consistent with observed active region properties in terms of Joy's law, the scatter of tilt angles about the average, the most frequently occurring tilt angle and the rotation rate of emerging loops with respect to the ambient plasma.

5.2 The Origin of Magnetic Twist and Chirality in Active Regions

Statistical tendencies for active regions to display signs (e.g. measurements of vertical current density) and symptoms (e.g. solar flares and eruptions) of magnetic twist in the solar atmosphere (Pevtsov et al. 1994, 2014; Wang 2013; Schmieder et al. 2014) offers clues that may help us rule out theories of the solar dynamo. An outstanding question is how active regions develop magnetic twist. Does the dynamo spawn flux concentrations that inherently have net twist? Or do the magnetic flux bundles develop twist as they rise through the convection zone or even as they erupt onto the surface? Finally, what is the relation between active region tilt and twist? First we briefly discuss ways by which magnetic twist is inferred from observations.

Once an active region has appeared at the solar surface, vector magnetograms can be used to probe the magnetic twist contained within the region. One commonly used quantity to characterize active region twist is the α parameter. Different definitions of α exist, and it is important to distinguish them

for the sake of clarity. For any general magnetic field, the field-line torsion parameter can be locally defined as $\alpha_{\rm torsion} = \mathbf{j} \cdot \mathbf{B} B^{-2}$, where $\mathbf{j} = \frac{c}{4\pi} \nabla \times \mathbf{B}$ is the current density. The sign of $\alpha_{\rm torsion}$ reflects the handedness of neighboring field lines gyrating around the local magnetic field. The magnetic field is locally right-handed (left-handed) if $\alpha_{\rm torsion} > 0$ (< 0). The amplitude of $\alpha_{\rm torsion}$ relates to the amount of twisting of the field.

Measurements of all three components of $\mathbf{B}$ are typically accessible only at a single height. More precisely, photospheric vector magnetograms sample magnetic fields in a limited range of optical depths near $\tau = 0.1$. Due to the corrugation of the surfaces of constant optical depth (e.g. the Wilson depression), this impacts the accuracy of the horizontal field gradients needed for computing j_z, a problem that is especially pronounced at small spatial scales. In any case, only the $j_z B_z$ contribution to the dot product in the definition of $\alpha_{\rm torsion}$ is accessible to observations. So a commonly used metric for the magnetic twist of active regions at the solar surface is $\alpha_z = j_z / B_z$ (e.g. Pevtsov et al. 1994; Leka et al. 1996; Leka & Skumanich 1999; Leka 1999). Here the dot product in the numerator has been replaced by $j_z B_z$ and B^2 in the denominator has been replaced by B_z^2, so one should recognize that α_z is *at best* a proxy for magnetic twist. The current helicity density H_c (e.g. Seehafer 1990) is related to field line torsion by the relation $H_c = \mathbf{j} \cdot \mathbf{B} = \alpha_{\rm torsion} B^2$.

Another proxy for magnetic twist is the force-free parameter $\alpha_{\rm FF}$. If the magnetic field is force-free, i.e. $\mathbf{j} \parallel \mathbf{B}$, then $\alpha_{\rm torsion}$ reduces to the force-free parameter. If the force-free field has the same value of α throughout the domain of interest, the field is called a linear force-free field and the associated twist parameter is $\alpha_{\rm LFF}$. Linear force-free fields are the solutions to the problem of minimizing the magnetic energy of the field subject to the imposed flux at the boundary and the constraint that magnetic helicity $\mathcal{H}_m$ be conserved (Woltjer 1958, also see discussion below for definition of $\mathcal{H}_m$). Observations reveal that α is usually not constant over an active region. $\alpha_{\rm best}$ refers to the linear force-free field solution such that the discrepancy between the observed horizontal field (equivalently, j_z) with the model horizontal field is minimized (Pevtsov et al. 1995).

The tilt of an active region should be distinguished from the magnetic twist within the region. The tilt is generally taken to be indicative of the large-scale ($L \gtrsim d$, where d is the footpoint separation between preceding and following polarities) handedness of the flux bundle associated with an active region, while magnetic twist (especially those flavors of α using local derivative operators) measures the handedness of the magnetic field at small scales ($L \lesssim d$). Joy's law concerning active region tilts indicates a preference for right- and left-handed active regions in the northern and southern hemispheres, respectively. As discussed later, AR tilt is possibly indicative of the magnetic writhe of a flux tube. This hemispheric preference is maintained even as the magnetic polarity reverses from one cycle to the next. In contrast, vector magnetogram observations of active regions show a preference for left- and right-handed magnetic twist within active regions located in the northern and

southern hemispheres, respectively. For example, Pevtsov et al. (1995) used the $\alpha_{\rm best}$ metric to measure the average twist in individual active regions.

As discussed in section 2.1, helioseismology has so far provided few direct probes of subsurface magnetic fields. However, knowledge about the flow structure in the solar interior offers some important clues. Local helioseismology reveals that, in the northern hemisphere of the Sun, divergent flows (associated with upwellings) are correlated with negative vertical vorticity ω_z and convergent flows (associated with downdrafts) are correlated with positive ω_z (Gizon & Duvall 2003; Langfellner et al. 2015, see Fig. 6). These results are consistent with the effect of the Coriolis force on the convective motions. In a local Cartesian frame in the northern hemisphere, $v_z\omega_z < 0$ for both upflows and downflows. Although the quantity $v_z\omega_z$ is only one component of the kinetic helicity $H_k = \mathbf{u}\cdot\nabla\times\mathbf{u}$, it nevertheless serves as a useful proxy for the sign of kinetic helicity in the turbulent solar convection. With respect to the sign of the mean kinetic helicity $\langle\mathbf{u}\cdot\nabla\times\mathbf{u}\rangle$, helioseismic results agree with theoretical (Rüdiger et al. 1999) and numerical calculations (Hathaway 1982; Ossendrijver et al. 2001) in that they suggest $\langle\mathbf{u}\cdot\nabla\times\mathbf{u}\rangle < 0$ in the northern hemisphere and $\langle\mathbf{u}\cdot\nabla\times\mathbf{u}\rangle > 0$ in the southern hemisphere.

Applying the model of Longcope & Klapper (1997) for twisted thin flux tubes (see brief discussion in section 5), Longcope et al. (1998) considered how initially untwisted flux tubes rising from the bottom of the convection zone may develop net twist as a consequence of their interaction with turbulence with non-vanishing kinetic helicity. In their model, the generation of net twist (as measured in terms of the magnetic pitch $q(l)$ averaged over the tube) is a purely geometrical effect that can be explained in terms of magnetic helicity. As pointed out by Woltjer (1958) and Moffatt (1969), the magnetic helicity of a system, defined as

$$\mathcal{H}_m = \int_V \mathbf{A}\cdot\mathbf{B}\; dV, \tag{1}$$

where $\mathbf{B} = \nabla\times\mathbf{A}$, is conserved under ideal MHD evolution when no magnetic flux crosses the boundary ∂V. For a set of closed rings of magnetic flux, as in the case of a global toroidal twisted flux tube, the magnetic helicity can be decomposed into contributions attributed to the writhe (denoted Wr) of the axis of the flux ring and the total twist of field lines around the axis (denoted Tw, see Berger & Field 1984; Moffatt & Ricca 1992). In this case,

$$\mathcal{H}_m = \frac{\Phi^2}{2\pi}(\mathrm{Tw}+\mathrm{Wr}) \tag{2}$$

where Φ is the magnetic flux of the tube. Longcope & Klapper (1997) pointed out that a flux tube with zero initial twist and writhe (hence zero magnetic helicity) can rise such that it develops net writhe due to buffeting by turbulent flows with non-vanishing mean kinetic helicity $\langle\mathbf{u}\cdot\nabla\times\mathbf{u}\rangle$. In their scenario, the interaction with turbulence is in terms of the drag on different portions of the rising tube, so the evolution satisfies ideal MHD. The helical motion of the ambient flows leads to a net writhe of the flux tube. Since $\mathcal{H}_m$ must

remain zero, magnetic twist of the same amplitude but opposite sign as writhe must result. The local generation of twist due to writhing of the tube is coined the Σ effect. Σ is the symbol used by Longcope et al. (1998) to denote the term that generates twist in time evolution equation of field line twist in the their thin flux tube model.

Based on theoretical expectations, Longcope et al. (1998) assumed $\langle \mathbf{u} \cdot \nabla \times \mathbf{u} \rangle$ to be negative (positive) in the northern (southern) hemisphere. As discussed earlier this expectation is consistent with helioseismic inferences (at least at supergranular scales, see Gizon & Duvall 2003; Langfellner et al. 2015). With this assumption, their model predicts $\mathrm{Wr} > 0$ (i.e. right-handed tilts of active regions) and $\mathrm{Tw} < 0$ (i.e. $\alpha_z < 0$) in the northern hemisphere. Longcope et al. (1998) argue that models relying on the α-effect (in the mean-field context, not to be confused with the magnetic twist parameter) would produce active regions with the same signs for Wr and Tw, which would be incompatible with empirical reports (e.g. Tian et al. 2001; Hagino & Sakurai 2004). This last claim deserves a bit of scrutiny. As demonstrated by Seehafer (1996), the α-effect produces magnetic helicity of opposite signs at the large and small scales. Consequently, the mean-field α-effect usually invoked to explain the tilts of active regions should generate small-scale twist of the opposite sign at sub-active region scales. So the tendency for $\mathrm{Tw} \times \mathrm{Wr} < 0$ does not, by itself, favor one picture over another.

6 Active Regions from Convective Dynamos

In section 5, we introduced various physical mechanisms that are deemed important for the birth of active regions. These effects include magnetic buoyancy, magnetoconvection, helical flows induced by the Coriolis force, angular momentum conservation, and magnetic helicity conservation. Due to the complexity of the problem, these effects have mostly been studied in isolation. For example, the convective flow patterns used in the thin flux tube models of Weber et al. (2011, 2013, see section 5.1) were purely hydrodynamic, so the work side-steps questions regarding the origin of toroidal flux tubes and the Lorentz force feedback of the magnetic field on the convection. The question of Lorentz force feedback is addressed in the 3D MHD models of flux tube rise by Fan (2008), Fan et al. (2013), Jouve & Brun (2009, 2013) and Pinto & Brun (2013). The numerical models in these studies solve the MHD equations in a spherical domain without resorting to the thin flux tube approximation. However, the flux tubes in these models are introduced in an ad hoc fashion.

Recent global turbulent dynamo simulations are beginning to capture all these effects in a self-consistent manner. Some of these models are starting to reproduce certain aspects of solar-like behavior. In particular, some dynamo calculations produce large-scale buoyant flux bundles that rise to the surface. An example of turbulent dynamo calculations generating large-scale bipolar structures is the work of Jabbari et al. (2015). In order to be able to control the degree by which helical and non-helical motions drive the dynamo, they

opted to not model convection, but instead imposed a forcing function in the momentum equation. They found that, by varying the latitudinal profile of the helical portion of the forcing function, they are able to generate bipolar active-region like structures in the mid-latitudes or in the polar regions. This result suggests the latitudinal shear profile in the Sun and Sun-like stars likely has an impact on the latitudes of activity belts.

The relation between helically-forced turbulence and rotationally affected thermal convection (as occurs on the Sun) is not straightforward. However, global convective dynamo models (with no externally prescribed forcing except for a chosen luminosity and background rotation rate) are also able to produce active-region scale flux concentrations. There are many unknowns about magnetoconvection in the high magnetic and dynamic Reynolds number, high density contrast regime of the solar convection zone. However, the solar luminosity is well measured and is not an adjustable parameter for a solar model. Since this paper is about solar active regions and is not intended to give an overview of convective dynamos, the following discussion will focus on models configured to transmit one solar luminosity ($L_\odot$).

The anelastic convective dynamo calculations by Nelson et al. (2011, 2013, 2014) for a model of a young Sun rotating at $\Omega = 3\Omega_\odot$ generate mean toroidal fields in the form of a pair of magnetic wreaths spanning the low to mid-latitudinal regions of the convection zone. (see Fig. 9). Convectively induced undulations of the wreaths spawn buoyant magnetic loops that rise toward the surface (see Fig. 10). The field strengths in the troughs of these undulations are roughly tens of kG, consistent with the field strengths of toroidal fields inferred from thin flux tube experiments (see section 5).

The global convective dynamo model of Fan & Fang (2014, 2015) of a star rotating at $\Omega_\odot$ reproduces solar-like differential rotation, yields super-equipartition field strengths (also tens of kG) near the bottom of the convection zone and generates buoyant flux bundles that rise toward the surface. Statistical analysis shows that the bundles are Hale/anti-Hale at a rate of 2.4:1. Hale-like bundles have a mean tilt of 7.5 ± 1.6 deg.

6.1 Lorentz force feedback by Active Region Magnetic Fields

An intriguing finding from the Fan & Fang (2014, 2015) study is that a purely hydrodynamic convection zone model yields anti-solar (fast poles and slow equator) differential rotation. This hints at the (possible) importance of the back reaction of the Maxwell stresses on the differential rotation profile.

The recognition that Maxwell stresses may modulate differential rotation is not new. Soon after the discovery of the torsional oscillation (a butterfly-like equatorward propagating pattern of zonal flow residuals relative to the temporally averaged differential rotation profile, see Howard & Labonte 1980, and chapter 9 of Howe, 2009), the Lorentz force has been invoked as a possible

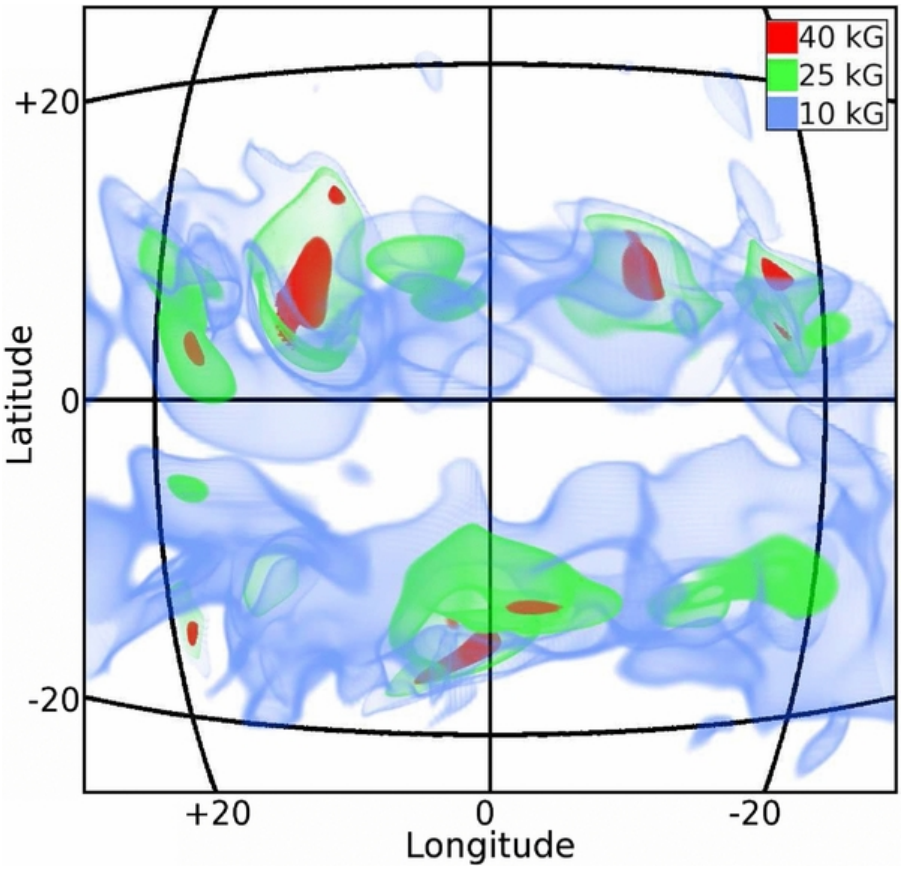

Fig. 9 Isosurface rendering of magnetic field strength in a convective dynamo simulation of a star rotating at $\Omega = 3\Omega_\odot$ by Nelson et al. (2013). Coherent toroidal magnetic wreaths are generated with field strengths beyond 10 kG. The magnetic wreathes contain cores that have superequiparition fields strengths reaching 45 kG.

driver of the oscillation (Schüssler 1981; Rempel 2007)[1]. However the strength of the "torsional oscillation" (zonal flows) in terms of rotation speed less than one percent of differential rotation. So if the Fan & Fang (2014, 2015) model were representative of the solar interior, their result hints at a more important role for Maxwell stresses than previously assumed.

Recent global dynamo simulations of a model star rotating at $\Omega = \Omega_\odot$ (Hotta et al. 2016) suggest that Lorentz force feedback from turbulent fields generated at the small-scales may even impact the strength of the large-scale toroidal field. At a magnetic Reynolds number $R_m \approx 300$ (with constant explicit values of the magnetic diffusivity η and viscosity ν), the dynamo generates coherent toroidal magnetic wreaths. For the same numerical resolution but with implicit

[1] Drivers of a thermal nature have also been investigated by Spruit (2003) and Rempel (2007).

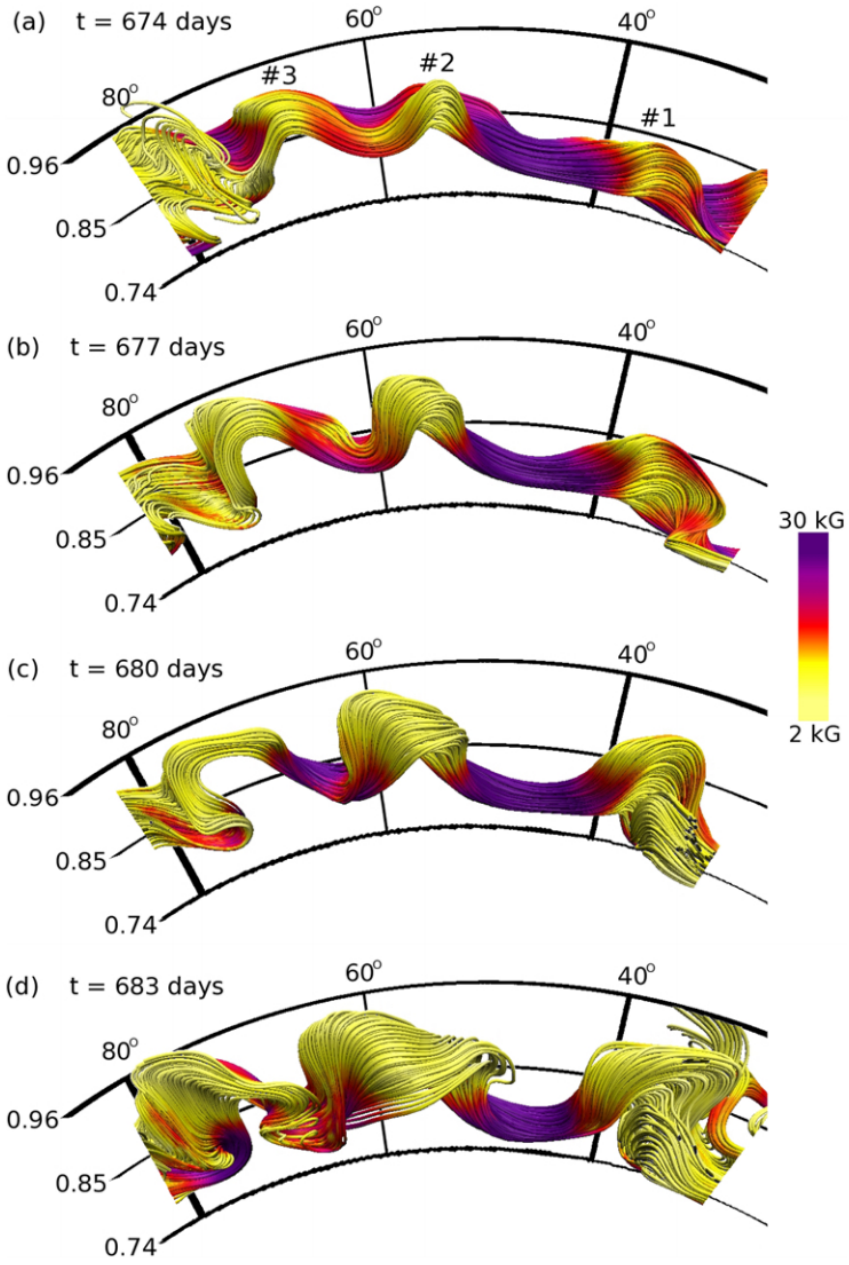

Fig. 10 Sequence of volume renderings of buoyant Ω-loops generated in the convective dynamo model of Nelson et al. (2014).

numerical diffusion set by a slope limiter scheme, the simulation becomes less diffusive, which increases the convective flow speeds at the small-scales. These stronger convective flows were found to have a destructive effect on the large-scale toroidal field. However, when the numerical resolution is increased even further such that $R_m \sim 2000$, the small-scale dynamo becomes efficient and the Lorentz-force feedback from the small-scale field dampens convective flows. This results again in a stronger large-scale toroidal field. In all three cases the large-scale toroidal field predominantly results from amplification by shear in the solar-like differential rotation profile and the poloidal field is amplified by convective turbulence. In short it is an $\alpha\Omega$ dynamo model. What this result demonstrates is that a large-scale field can persist (and as shown in Hotta et al. 2016, exhibit reversals) even in the presence of a small-scale dynamo if the latter is sufficiently efficient to have a strong Lorentz-force feedback.

Models where the interactions of the small and the large-scale fields are treated in a unified system are still in their infancy. There is at present no indication of convergence of the solutions with respect to magnetic and hydrodynamic Reynolds numbers. In particular, simulations have a tendency to operate in a regime where both Reynolds number are very similar, a regime that is known to favor turbulent dynamo action (see Tobias et al. 2013). The convective zone of the Sun is, however, in a very different regime where the dynamic Reynolds number overwhelmingly exceeds the magnetic one (in other words the magnetic Prandtl number $Pr = \eta/\nu \ll 1$). Under these circumstances the nature of the turbulently driven dynamo action is not yet well understood (see Martínez Pillet 2013, and references therein; see also Thaler & Spruit, 2015). On the other hand, all current numerical simulations of convective dynamos in the solar context are effectively large-eddy simulations where the smallest captured scales for both magnetic and velocity fields are far removed from the theoretical dissipation scales. It is unclear what the appropriate subgrid models for magnetic and viscous dissipation are and, given the appropriate models, whether they result in an effective Pr regime equivalent to that expected from atomic values of the diffusivities. However it is clear that a potential coupling between the two dynamos can be essential for advancing our understanding of the origin of active regions on the Sun.

7 Emergence and Active Life of AR Magnetic Fields

Having discussed the subsurface genesis and evolution of active region magnetic fields, we briefly turn to the next phase of their life cycle, namely emergence and development at and above the solar surface.

The evolutionary state of an AR is closely related to the level of magnetic activity it produces, *i.e.* the frequency and importance of flares and coronal mass ejections. For ARs that are flare productive, larger flares (*i.e.* above the C-class) are produced as long as high magnetic flux density/strong magnetic field concentrations are present, and the overall flare production rate decreases sharply with decreasing flux density, while the rate of CME pro-

duction shows a much slower decrease with time, i.e. CMEs keep erupting from active regions well into their decay phase (van Driel-Gesztelyi & Green 2015). This is not surprising, as during the decay phase persistent flux cancellations along inversion lines occur (Green et al. 2011). This is taken as an observational signature of flux rope generation, either, through reconnection and submergence of sheared field lines (van Ballegooijen & Martens 1989) or via flux emergence (MacTaggart & Hood 2010). A prerequisite for sustained CME production is maintained magnetic shear or helicity in the active region field and sufficient amounts of flux cancellations. As CMEs consume magnetic free energy and carry away magnetic helicity, they exhaust this reservoir.

As an example, Cheung & DeRosa (2012) constructed time-dependent magnetofrictional coronal field models of AR 11158 by using SDO/HMI line-of-sight magnetograms. Magnetofriction assumes the plasma velocity in the induction equation to be parallel to the Lorentz force (Yang et al. 1986). By varying a shearing parameter that controls energy injection, they report that persistent shearing/twisting near the polarity inversion line is required to generate serial flux rope ejections. By using time sequences of *vector* magnetograms as well as surface flow maps from Doppler measurements and local correlation tracking, it is now possible to derive the full photospheric electric field of emerging and developing active regions. This allows one to quantify the fluxes of magnetic energy and relative helicity (Kazachenko et al. 2014, 2015) from the solar interior to the corona. Electric fields derived in this way have also been used to drive a magnetofrictional model of AR 11158 over a 5-day period (Fisher et al. 2015, see Fig. 11).

For an extensive review of active region evolution (during the phase when they are visible at and above the photosphere), we encourage the reader to consult van Driel-Gesztelyi & Green (2015). For discussions of the detailed processes related to magnetic flux emergence, we refer the reader to reviews by Schmieder et al. (2014) and Cheung & Isobe (2014).

8 Ageing Active Regions

After the brief period of flux emergence, which lasts for up to five days, depending on the total flux to be emerged, starts the decay phase of active regions, which is at least an order of magnitude longer. How long it takes for the emerged flux to disperse to a quiet-sun magnetic flux density level while being removed by magnetic cancellation, depends on the (i) total magnetic flux (size) of the active region, (ii) level of magnetic activity outside and (iii) magnetic complexity within the active region. During high activity periods large active regions may become indistinguishable from the "background" magnetic field within four months, while during solar minima that may take as long as 10 months (Schrijver & Harvey 1994).

During the dispersion process the area of the active region has an approximate linear growth (van Driel-Gesztelyi et al. 2003), while the fields are more and more effectively shaped by differential rotation, rotating the polar-

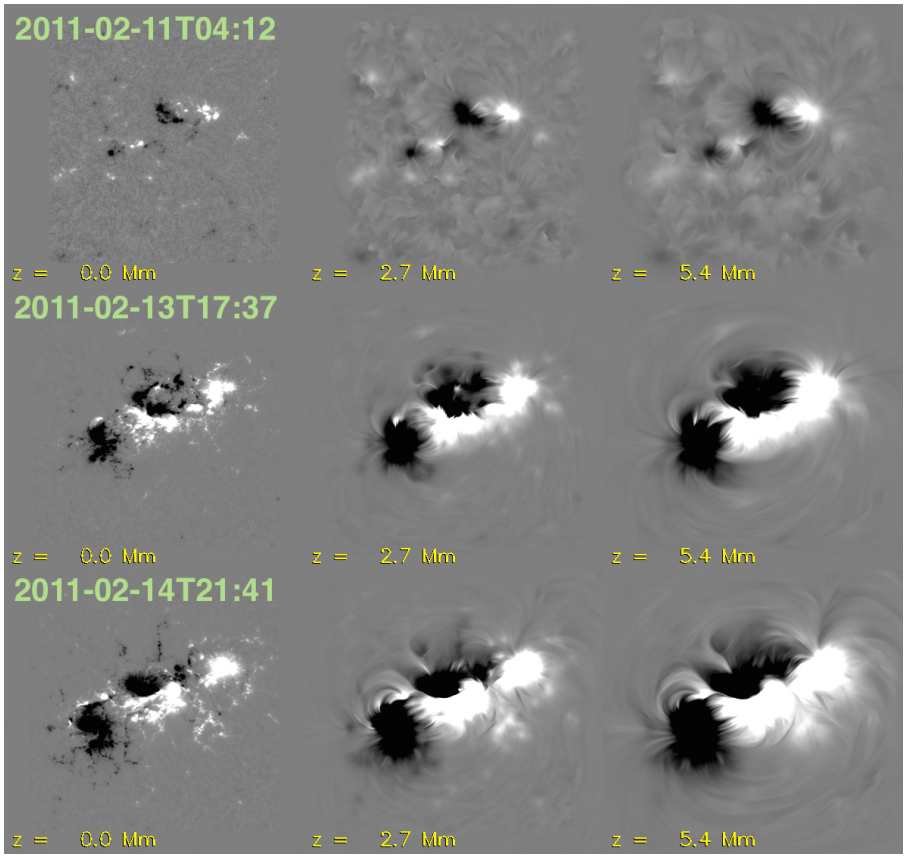

Fig. 11 Distribution of B_z at photospheric ($z = 0$ Mm), chromospheric ($z = 2.7$ Mm) and coronal heights ($z = 5.4$ Mm) of a data-driven model of NOAA AR 11158 (images produced from simulation data described in Fisher et al. 2015). The data-driven time dependent model retains information about the emergence history. Early in its evolution (see snapshot at 2011-02-11T04:12), the AR consists of two isolated bipolar regions. As the two bipolar regions grow, the following polarity of one (to the west) jousts against the leading polarity of the other and creates a sheared polarity inversion line.

ity inversion line clockwise in the south, and counter-clockwise in the north hemisphere. However, the weighted polarity separation may not be affected by the dispersion (Li & Welsch 2008). Differential rotation shears the dispersing fields, i.e. injects magnetic helicity (DeVore 2000). However, the helicity injection is not a monotonous function of time. Once the magnetic inversion line has rotated to 45^o with respect to the equator, the sign of helicity injection by differential rotation will change, and at any larger angle (i.e. more parallel to the equator) the accumulated helicity will be eroded and even reversed by this process. Démoulin et al. (2002) estimated a total magnetic helicity of 8.3×10^{42} Mx^2 produced by differential rotation during a five-month period in AR 7978, which would only supply enough helicity for 4 CMEs, while the

AR 7978 produced 28 CMEs during this period (see Table 6 & 7 in van Driel-Gesztelyi & Green (2015). Démoulin et al. (2002) concluded that for AR 7978, which decayed in isolation, differential rotation was not the major source of magnetic helicity injection.

Removal of magnetic flux takes place by magnetic cancellation (Martin et al. 1985), which it is thought to reflect, in the majority of the cases, small-scale submergence of flux. There is an asymmetry between flux submergence and its counterpart, flux emergence, that is worth noticing. Flux emergence at all scales has a well-defined observational signature, namely fields parallel to the solar surface harbouring upflows. They have been detected in the large scale emergence of active regions (see Fig. 3 of Lites et al. 1998) and during the surfacing of small scale loops brought up by granules (see Figs. 5 and 6 of Guglielmino et al. 2010). The opposite, flux submergence detected as fields parallel to the solar surface in a downflow region is more scarce (but see Chae et al. 2004) and it has always a localized patchy nature. Submergence can be brought along by downward magnetic tension forces in high-curvature small-scale loops created in low-atmospheric magnetic reconnection (Cheung et al. 2008; Cameron et al. 2011). In cancellation processes opposite polarity flux concentrations approach each other, and an equal amount of flux disappears from each polarity. The main cancellation sites are along the magnetic inversion lines within the active region and along its external boundaries. In the latter case, submergence is expected to have the observed patchy nature as it will depend on the neighboring fields that are randomly encountered as the active region flux disperses. By contrast, along the active region neutral line, the systematic cancellation processes observed during the decay phase have not yet been unequivocally demonstrated to represent submergence episodes. Indeed the most detailed study of the transverse fields observed at an active region neutral line, concluded that these field lines display large scale upflows of a few hundreds meters per second (see Kuckein et al., 2012; see also the discussion in Mackay, 2015). It is clear that the nature of the cancellation processes at active region neutral lines urgently needs further investigation.

Magnetic complexity within the active region naturally increases the magnetic cancellation rate, resulting in the survival of the majority polarity locally. Such cancellation processes effectively wipe out complexity within an ageing active region, leading to a simplification of the magnetic structure, establishing a pair of opposite-polarity monopolar regions. Small-scale flux emergence episodes within either polarity may take place, but as long as the emerging flux is inferior to the flux of the ageing active region, complexity is only temporarily introduced. As such secondary flux emergence episodes are expected to bring up equal amounts of positive and negative fluxes (although see Wang & Shi 1993; Yardley et al. 2016, for examples when does not appear to be the case) and cancellation processes between the ageing and new flux remove equal amount of fluxes, these smaller-scale flux emergence episodes only temporarily increase the total flux present.

A number of detailed case studies indicate that active regions have flux loss rates in the range $5 \times 10^{19} - 5 \times 10^{20}$ Mx day^{-1}. Green et al. (2011)

reported a flux loss rate of 2×10^{20} Mx day^{-1}, corresponding to a relative loss rate of $\dot{\Phi}/\Phi = -0.1$ day^{-1}, where Φ is half of the total unsigned flux. At such a rate the active region would not last longer than 10 days and so is unlikely to contribute significantly to the polar flux budget. However, Wang et al. (1989, see their Fig. 3) measured the flux decay of an active region over 4 solar rotations and obtained a rate of 5×10^{19} Mx day^{-1}, a much reduced value. Dalda & Martinez Pillet (2008) measured a flux decay rate of 4×10^{20} Mx day^{-1} for a period of about 2.5 days that was followed by a plateau where the remaining flux evolved at a much slower pace. A similar curve, including a plateau region, was found by Sterling et al. (2010, see their Fig. 6). Tentatively, one would conclude that there is a flux decay phase of active regions that occurs at a pace of several 10^{20} Mx day^{-1} and that acts upon only a fraction of the total flux of the active region. For the case studied by Dalda & Martinez Pillet (2008), they estimated this to be about 50-70% of the total active region flux. The remaining portion of the flux disappears at a much slower pace, perhaps at a rate compatible with the decay measured by the diffusion processes as obtained by Wang et al. (1989, basically one order of magnitude slower). It is worth noting that morphological changes in the spatial flux distribution of an active region (e.g. spots disintegrating into small-scale magnetic features) can complicate flux loss measurements. This due to the temperature-sensitivity of the Stokes profiles of some spectral lines. So one may detect apparent flux changes even though the flux has only been redistributed (flux "vanishing in situ"). In any case studies of the flux loss rates of a large sample of active regions is critically needed.

In some cases, unsual sunspot motions may occur, possibly owing to non-Ω-loop (e.g. U-loop, see van Driel-Gesztelyi et al. 2000) subsurface geometry, or multiple major flux emergence episodes in an active region, which drive large flux concentrations towards the internal inversion line, significantly increasing the cancellation rates there (Yardley et al. 2016). The presence of active regions in the vicinity of emerging flux, if they are favorably oriented, can lead to increased cancellation rates along the external boundaries and shortened active-region lifetimes. High decay rates have indeed been measured in complex active regions where not only small flux concentrations but spot-size magnetic fields cancel (e.g. 5×10^{20} Mx day^{-1} cancellation rate found in AR 11226 by Yardley et al., 2016; see also Sterling et al., 2010).

Magnetic flux cancellation along magnetic inversion lines do not only remove flux, but also change the overall magnetic topology of the ageing active region. Through these processes, magnetic shear is getting gradually converted into twist, forming a flux rope along the magnetic inversion line (van Ballegooijen and Martens, 1989), and redistributing helicity (from small to large scales, see Mackay et al. 2014), concentrating it along the inversion line, which explains the gradient in force-free alpha found in active regions (Schmieder et al. 1996). Not all the cancelled flux is built in the forming flux rope, however, while the shear is transformed into twist. Green et al. (2011) very clearly show (see their Figure 11) how cancellations in a five-fieldline sheared arcade would form a two-fieldline flux rope, whose footpoints had no opposite-polarity

cancelling partners in the interior of the arcade. This suggests that the more sheared the arcade is the more flux can be built in the flux rope. At the opposite end of the scale, no flux rope forms in a potential arcade where each flux concentration has an opposite polarity with which to cancel. Savcheva et al. (2012) shows that most models are compatible with 60–70 % of the cancelled flux and 30–50 % of the total flux of a sheared active region being equal to the sum of toroidal (parallel to flux rope axis) and poloidal (transverse to flux rope axis) fluxes of flux ropes built up this way.

There exists a number of surface flux transport (SFT) models aiming to explain how active regions decay and how their magnetic flux disperses over the solar surface. SFT models treat the transport of radial magnetic flux on the solar surface due to advection by differential rotation and meridional circulation and by turbulent diffusion. For a comprehensive review, we refer the reader to papers in this volume by Cameron et al. (2016) and by Wang & DeRosa (2016) and the Living Reviews paper by Mackay & Yeates (2012). SFT modelers have had considerable success in applying models to explain the processes by which magnetic flux in the polar caps build up and subsequently reverse. The tilt of active regions is key to this. Due to Faraday's law (resulting in the conservation of magnetic flux), there are two ways to create net residual flux in a hemisphere. The first is for transport of flux across the equator. Due to Joy's law, trailing polarity spots are, on average, found at higher latitudes while leading polarities are found at lower latitudes. The flux from leading polarities is more likely to be transported across the equator, which results in residual flux from the trailing polarities to be transported toward the polar regions by meridional circulation and diffusion.The second way is to have tilted active regions emerge such that they straddle the equator.

SFT models are kinematic, which neglects the back reaction of the Lorentz force on flows. Furthermore, 2D SFT models do not take into account the 3D nature of active regions. For developing physical insight into how active regions may decay, one must resort to 3D radiative MHD simulations. Rempel & Cheung (2014) carried out a number of active region emergence and decay experiments by advecting semi-toroidal flux tubes through the bottom boundary of their Cartesian domain, which is located at 15.5 Mm below the photosphere. In their models the numerical resolution and the top boundary conditions were chosen such that the model active regions only developed naked spots. They examined the rate of flux dispersal for one of the model spots in the first two days during the decay phase and found it to be consistent with 2D diffusion with turbulent diffusivity $\eta_{\rm turb} = 350$ km^2 s^{-1}.

Rempel (2015) carried out 3D radiative MHD simulations of isolated sunspots (see Fig. 12). For an experiment where the top boundary condition enforces a potential magnetic field, the model spot has only very short, rudimentary penumbral filaments. It is almost 'naked'. For a numerical experiment with the same initial conditions but with a top boundary condition that forces the field to be more inclined to the vertical (so that the horizontal field is twice as strong compared to a potential field), the umbra is surrounded by a penumbra. For the naked spot, Rempel (2015) reports a flux decay rate of roughly

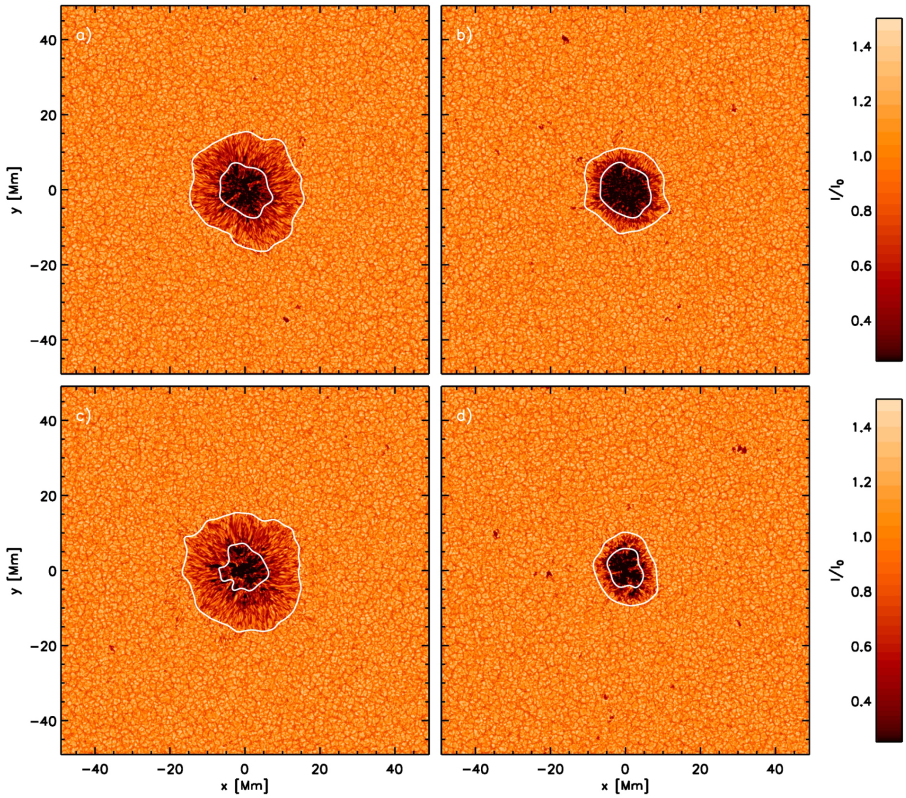

Fig. 12 3D radiative MHD simulations of sunspots with and without a penumbra (from Rempel 2015). Panels (a) and (c) show the brightness intensity of a model sunspot with a penumbra separated in time by 50 hr. This model was run with a top boundary condition that enforces the horizontal field to be more inclined than a potential field. Panels (b) and (d) show a corresponding model for a sunspot with rudimentary penumbra, which was run with a potential field top boundary condition. The latter decays at a rate of 10^{21} Mx day^{-1} whereas former is essentially stable.

10^{21} Mx day^{-1}. In comparison, the sunspot with penumbra maintains its flux content over the same period of a few days. He analyzed the flow structure around the two spots and found that the filling factor of downflows in the periphery of the spot is suppressed in the case of the spot with a fully-fledged penumbra. This reduces the flux loss due to downward pumping of magnetic flux, and keeps the sunspot coherent for longer.

Consider a sunspot in a real active region on the Sun. The sunspot resides within an active region, which itself may be located in the vicinity of other active regions. Due to existing magnetic connectivities between the spot and surrounding polarities, the relaxation of the chromospheric and coronal field above the spot is not unconstrained and is unlikely to be in the lowest energy potential state. Instead the field will be closer to a non-linear force-free, current-carrying state. The results of Rempel (2015) gives some physical

grounding to the idea that chromospheric and coronal complexity may have an impact on the underlying sunspot in terms of photospheric magnetic field and penumbral structure. And if the presence of a penumbra helps stabilize a spot from decay, it would suggest that the the coronal field configuration may have some influence on the decay process of sunspots and active regions. These are speculations that can be tested by analysis of observations and by further numerical modeling.

9 Closing (the loop) remarks

Statistical studies of the properties of active regions and ephemeral regions (e.g. frequency, latitude and orientation of emergence) suggest that the two features are drawn from a broad spectrum of magnetic structures generated within the solar interior. The existence of magnetic bipoles down to the scales of granulation provides evidence for the operation of a small-scale dynamo in addition to the large-scale dynamo. But the 'two' dynamos are not decoupled. The continuous distribution of bipole sizes motivates the search for a unified physical model to explain both active regions and smaller magnetic bipoles.

Helioseismology has so far not provided direct constraints on the strengths and geometries of active regions before they emerge. However, helioseismic characterization of flows in the solar interior gives indirect hints as to how active regions are generated and transported. For instance, the differential rotation profile in radius and latitude provides a constraint on convection and magnetoconvection models. In addition, the measurement of the kinetic helicity in the two hemispheres reveals how convective flows at supergranular scales introduce twist and writhe into rising flux tubes. There is empirical evidence that active regions exhibit opposite signs of small-scale twist and large-scale writhe (the latter in terms of tilt). Buffeting of the active region by convective flows introduces negative (positive) twist in the northern (southern) hemisphere and the flux bundle can as a result develop a writhe of the opposite sign. This is consistent with magnetic helicity conservation.

Both simple thin flux tube models and state-of-the-art global convective dynamo models suggest active regions begin their rise to the surface as superequipartition (tens of kG) strength magnetic bundles lying deep in the solar interior (bottom half of the convection zone).

The most recent global convective dynamo calculations (Nelson et al. 2011; Fan & Fang 2014; Hotta et al. 2016) yield toroidal magnetic wreaths amplified by differential rotation within the convection zone. Despite the apparent success of recent models, one should still be cautious about their fidelity to the Sun. Although convective dynamo models are starting to reproduce some solar-like properties, there remains a number of outstanding issues. In several models, different choices of diffusivities (viscous, thermal and magnetic) and numerical resolutions can yield qualitatively vastly different results (e.g. Nelson et al. 2013; Fan & Fang 2014; Hotta et al. 2016) in terms of the strength of the mean and maximum subsurface toroidal fields generated by the dynamo.

Furthermore, several hydrodynamic (Brown et al. 2008; Fan & Fang 2014) and magnetohydrodynamic (Fan & Fang 2014; Hotta et al. 2016) models are tuned so that a large fraction (about one third in the middle of the convection zone) of the outward energy flux is carried by radiative/thermal diffusion as opposed to enthalpy transport (i.e. positive correlations between temperature fluctuations and radial flows). The enhancement of thermal diffusion suppresses the otherwise large convective r.m.s. velocities, which in turn reduces the Reynolds stress transport of angular momentum to the poles. This artificial suppression of the Reynolds stress is generally recognized as a practical device to obtain solar-like differential rotation (slow poles and fast equator). For the time being this remains an ad hoc choice for a sub-grid model of energy transport. The implications of this sub-grid model for our understanding of solar magnetoconvection remain unclear.

The aforementioned generation of global solar dynamo models do not include the tachocline nor the near surface shear layer (see Fig. 2), which are the regions of strongest shear in the solar interior. Such models can be contrasted with earlier older models where the tachocline (e.g. Dikpati & Gilman 2001) or the near surface shear layer (Brandenburg 2005) act as primary agents of the Ω-effect and/or as the reservoir for field storage (e.g. Browning et al. 2006). Even without the tachocline and near surface shear layer the dynamo models are able to yield active region-like buoyant magnetic bundles. However they do not produce quasi-periodic reversals with solar-like butterfly diagrams. So the roles of the neglected shear layers remain unknown.

The buoyant flux bundles generated in the convective dynamo models do not rise through the surface to become compact active regions harboring sunspots. The primary reason is that the simulation domains do not capture the top twenty or so Mm (about half of the total pressure scale heights) of the convection zone. There are separate Cartesian MHD models of emerging active regions that capture those near-surface layers (Cheung et al. 2010; Stein & Nordlund 2012; Rempel & Cheung 2014), but the large-scale emerging fields in those models are imposed in an ad hoc fashion (by specifying certain bottom boundary conditions). The goal for future models is to connect this divide and to capture the formation, development and decay of active regions.

Surface flux transport models of active regions subject to differential rotation, turbulent diffusion and meridional circulation achieve considerable success in reproducing the migration of flux to the high latitudes to cause reversals of the large-scale poloidal field (refer to companion review papers in this volume by Cameron et al. and by Wang & DeRosa). How similar patterns of magnetic flux migration occur in the solar interior is less well known. The model of van Ballegooijen & Mackay (2007) treats the evolution of magnetic field in both the convection zone and corona in a simplified fashion. The coronal field evolves by magnetofriction (i.e. setting $\mathbf{v} \propto \mathbf{j} \times \mathbf{B}$ in the induction equation). The kinematically imposed flows in the model interior mimic (1) downward pumping by convection and (2) the ideal buoyant rise of a section of a toroidal flux tube. In this model, an Ω-loop is made to emerge to create an active region with flux expanding into the corona. Subsequent flux cancel-

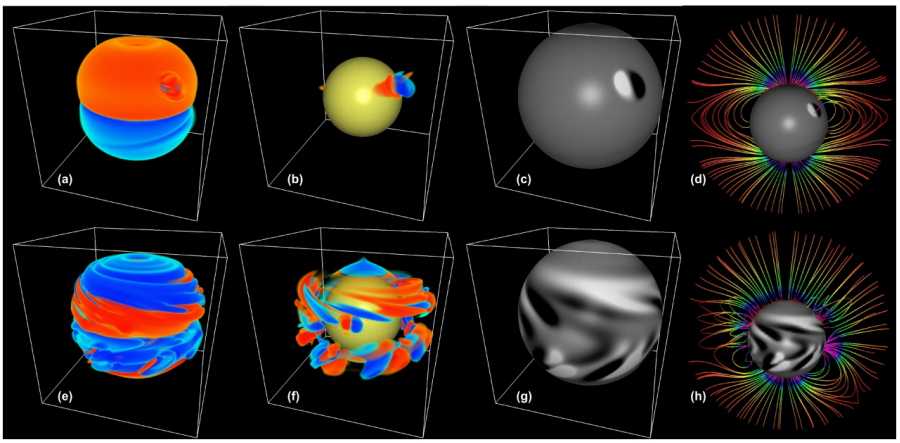

Fig. 13 3D data-driven Babcock-Leighton flux transport model by Yeates & Muñoz-Jaramillo (2013). The top (bottom) row shows visualizations near solar minimum (maximum). Panels in the first and second columns (from the left) show 3D renderings of the toroidal and poloidal components of the subsurface magnetic field, respectively. Panels in the third column shows the radial field at $r = R_\odot$ (saturated at $B_r = \pm 25$ G). Panels in the fourth column show potential field source surface extrapolations.

lation at the photospheric polarity inversion line leads to the formation of a flux rope that erupts due to loss of equilibrium. Associated with this is the submergence of flux back into the convection zone, which results in the repair of the original toroidal belt.

In this description of active region evolution, the final fate of the field lines is to submerge and return to their original state inside the Sun. But elsewhere in this paper we have described how some of the active region flux is known to be dispersed through the action of meridional circulation and diffusion, a critical process for the solar dynamo that leads to the reversal of the polar fields. This brings up the question of what fraction of the active region magnetic flux, if any, submerges and repairs the toroidal tube and what fraction is transported to the poles. One would also need to understand what distinguishes the two types of field lines: is the fraction of flux that participates in the diffusion process the one that somehow got disconnected from below and the fraction that submerges the one that is still tightly rooted to the deep interior? At any rate, it is unclear if the two processes co-exists during the decay phase of an active region and an effort must be made to understand if this is the case. Some indication for the co-existence of these two processes comes from the comparison of historical values of decay rates. Flux losses from recurrent active regions that are known to contribute to the polar reversal are hard to quantify as it is difficult to identify the amount of flux that belongs to the active region in each rotation.

Yeates & Muñoz-Jaramillo (2013) extended the solar interior kinematic model of van Ballegooijen & Mackay (2007) to perform a data-driven 3D Babcock-Leighton flux transport model of a solar cycle (see also Miesch & Dik-

pati 2014). They prescribed subsurface flows designed to advect toroidal flux onto the surface. Idealized bipolar emergences were imposed at the times and locations (latitudes and longitudes) of large bipolar magnetic regions ($\Phi \geq 10^{22}$ Mx) spotted in Kitt Peak synoptic magnetograms during the years 1996 to 2008. The prescribed plasma expansion in the loops corresponds to an effective density contrast of 27 between the bottom of the convection zone and the photosphere. This is somewhat unrealistic since the actual density contrast in the Sun is 10^6. Nevertheless, the model is calibrated to yield bipolar magnetic regions at $r = R_\odot$ to have statistical properties similar to observed ones (e.g. tilts). The key advantage of this data-driven model is that it provides the 3D distribution of the subsurface magnetic field at different times of the cycle (see Fig. 13). This model includes downward turbulent pumping (as a prescribed background flow) and captures the toroidal belt repair mechanism proposed by van Ballegooijen & Mackay (2007). The model also includes differential rotation, which is the primary mechanism for toroidal field amplification. By virtue of being a kinematic model, it cannot be used to address questions regarding the structural stability of the toroidal belts. But recall that global convective dynamo calculations yield persistent toroidal magnetic wreathes pervading the mid- to low convection zone.

The range of measured loss rates of magnetic flux from active regions ($5 \times 10^{19} - 5 \times 10^{20}$ Mx day^{-1}) quoted in section 8 are based on a few studies and need to be confirmed over a larger number of active regions. If the faster decay rates are associated with the cancellation at the neutral line, the importance of any potential flux repairing mechanism can be quantified. The flux that decays at a much slower pace would be the only one that remains available for surface transport processes to reverse the polar fields. Thus studying the flux history of a statistically significant number of active regions and the dynamics at the neutral line can prove crucial to understand the key players in the last phases of the evolution of an active region. Note that persistent submergence of active region flux and repairing of the toroidal tubes cannot continue beyond the corresponding solar cycle, thus raising the question about how the toroidal flux of a given cycle is finally destroyed. One option is the encounter of the two oppositely directed toroidal belts in each hemisphere near the equator where they would annihilate. Another important mechanism may be the unwinding of the toroidal field due to the reversal of the poloidal field. In any case, understanding which processes are key for closing the solar dynamo loop in its final stages requires first to detect the existence of any flux repairing mechanism and the dynamics of the magnetic fields at the neutral line of active regions. The answers to these questions may be key to closing the loop on the life cycle of active region magnetic fields.

Acknowledgements MCMC is supported by NASA's SDO/AIA contract (NNG04EA00C) and grant (NNX13AJ96G) to LMSAL. AIA is an instrument onboard the Solar Dynamics Observatory, a mission for NASA's Living With a Star program. Part of this paper was written while MCMC was a Visiting Associate Professor at the National Astronomical Observatory of Japan (NAOJ) in Tokyo. MCMC wishes to thank his NAOJ hosts, especially

Professor Shin Toriumi, for their excellent hospitality. LvDG acknowledges the Hungarian Scientific Research Fund (OTKA) for support through grant no. K-109276. The National Solar Observatory is operated by AURA, Inc. under a cooperative agreement with the National Science Foundation. The National Center for Atmospheric Research is sponsored by the National Science Foundation. Finally, the authors wish to thank the anonymous referee for very constructive feedback.

References

Altschuler, M. D., & Newkirk, G. 1969, Solar Phys., 9, 131
Babcock, H. W. 1961, Astrophys. J., 133, 572
Belucz, B., Dikpati, M., & Forgács-Dajka, E. 2015, Astrophys. J., 806, 169
Berger, M. A., & Field, G. B. 1984, J. Fluid Mech., 147, 133
Brandenburg, A. 2001, Astrophys. J., 550, 824
—. 2005, Astrophys. J., 625, 539
Brown, B. P., Browning, M. K., Brun, A. S., Miesch, M. S., & Toomre, J. 2008, Astrophys. J., 689, 1354
Browning, M. K., Miesch, M. S., Brun, A. S., & Toomre, J. 2006, Astrophys. J. Lett., 648, L157
Buehler, D., Lagg, A., & Solanki, S. K. 2013, Astron. Astrophys., 555, A33
Caligari, P., Moreno-Insertis, F., & Schüssler, M. 1995, Astrophys. J., 441, 886
Caligari, P., Schüssler, M., & Moreno-Insertis, F. 1998, Astrophys. J., 502, 481
Cameron, R., Vögler, A., & Schüssler, M. 2011, Astron. Astrophys., 533, A86
Centeno, R., Socas-Navarro, H., Lites, B., Kubo, M., Frank, Z., Shine, R., Tarbell, T. D., Title, A. M., Ichimoto, K., Tsuneta, S., Katsukawa, Y., Suematsu, Y., Shimizu, T., & Nagata, S. 2007, Astrophys. J. Lett., 666, L137
Chae, J., Moon, Y.-J., & Pevtsov, A. A. 2004, Astrophys. J. Lett., 602, L65
Chen, P. F. 2011, Living Rev. Solar Phys., 8
Cheung, M. C. M., & DeRosa, M. L. 2012, Astrophys. J., 757, 147
Cheung, M. C. M., & Isobe, H. 2014, Living Rev. Solar Phys., 11, 3
Cheung, M. C. M., Rempel, M., Title, A. M., & Schüssler, M. 2010, Astrophys. J., 720, 233
Cheung, M. C. M., Schüssler, M., & Moreno-Insertis, F. 2007, Astron. Astrophys., 467, 703
Cheung, M. C. M., Schüssler, M., Tarbell, T. D., & Title, A. M. 2008, Astrophys. J., 687, 1373
Choudhuri, A. R. 1989, Solar Phys., 123, 217
—. 1990, Astron. Astrophys., 239, 335
Choudhuri, A. R., & D'Silva, S. 1990, Astron. Astrophys., 239, 326
Choudhuri, A. R., & Gilman, P. A. 1987, Astrophys. J., 316, 788
Christensen-Dalsgaard, J., Gough, D. O., & Thompson, M. J. 1991, Astrophys. J., 378, 413
Dalda, A. S., & Martinez Pillet, V. M. 2008, in Astronomical Society of the Pacific Conference Series, Vol. 383, Subsurface and Atmospheric Influences on Solar Activity, ed. R. Howe, R. W. Komm, K. S. Balasubramaniam, & G. J. D. Petrie, 115
Danilovic, S., Beeck, B., Pietarila, A., Schüssler, M., Solanki, S. K., Martínez Pillet, V., Bonet, J. A., del Toro Iniesta, J. C., Domingo, V., Barthol, P., Berkefeld, T., Gandorfer, A., Knölker, M., Schmidt, W., & Title, A. M. 2010a, Astrophys. J. Lett., 723, L149
Danilovic, S., Schüssler, M., & Solanki, S. K. 2010b, Astron. Astrophys., 513, A1
De Pontieu, B. 2002, Astrophys. J., 569, 474
Démoulin, P., Mandrini, C. H., Van Driel-Gesztelyi, L., Lopez Fuentes, M. C., & Aulanier, G. 2002, Solar Phys., 207, 87
DeVore, C. R. 2000, Astrophys. J., 539, 944
Dikpati, M., & Gilman, P. A. 2001, Astrophys. J., 559, 428
Domínguez Cerdeña, I., Sánchez Almeida, J., & Kneer, F. 2003, Astron. Astrophys., 407, 741
D'Silva, S., & Choudhuri, A. R. 1993, Astron. Astrophys., 272, 621
Fan, Y. 2004, Living Rev. Solar Phys., 1
Fan, Y. 2008, Astrophys. J., 676, 680

—. 2009, Living Rev. Solar Phys., 6
Fan, Y., & Fang, F. 2014, Astrophys. J., 789, 35
—. 2015, ArXiv e-prints: 1512.08038
Fan, Y., Featherstone, N., & Fang, F. 2013, ArXiv e-prints: 1305.6370
Fan, Y., Fisher, G. H., & Deluca, E. E. 1993, Astrophys. J., 405, 390
Fan, Y., Fisher, G. H., & McClymont, A. N. 1994, Astrophys. J., 436, 907
Ferriz-Mas, A., & Schüssler, M. 1993, Geophysical and Astrophysical Fluid Dynamics, 72, 209
—. 1995, Geophysical and Astrophysical Fluid Dynamics, 81, 233
Fisher, G. H., Abbett, W. P., Bercik, D. J., Kazachenko, M. D., Lynch, B. J., Welsch, B. T., Hoeksema, J. T., Hayashi, K., Liu, Y., Norton, A. A., Dalda, A. S., Sun, X., DeRosa, M. L., & Cheung, M. C. M. 2015, Space Weather, 13, 369
Fisher, G. H., Fan, Y., & Howard, R. F. 1995, Astrophys. J., 438, 463
Giles, P. M. 2000, PhD thesis, Stanford University
Gizon, L., & Duvall, Jr., T. L. 2003, in ESA Special Publication, Vol. 517, GONG+ 2002. Local and Global Helioseismology: the Present and Future, ed. H. Sawaya-Lacoste, 43–52
Gosling, J. T. 1993, J. Geophys. Res., 98, 18937
Gošić, M., Bellot Rubio, L. R., Orozco Suárez, D., Katsukawa, Y., & del Toro Iniesta, J. C. 2014, Astrophys. J., 797, 49
Granzer, T., Schüssler, M., Caligari, P., & Strassmeier, K. G. 2000, Astron. Astrophys., 355, 1087
Green, L. M., Kliem, B., & Wallace, A. J. 2011, Astron. Astrophys., 526, A2
Greer, B. J., Hindman, B. W., Featherstone, N. A., & Toomre, J. 2015, Astrophys. J. Lett., 803, L17
Guglielmino, S. L., Bellot Rubio, L. R., Zuccarello, F., Aulanier, G., Vargas Domínguez, S., & Kamio, S. 2010, Astrophys. J., 724, 1083
Haber, D. A., Hindman, B. W., Toomre, J., Bogart, R. S., Larsen, R. M., & Hill, F. 2002, Astrophys. J., 570, 855
Hagenaar, H. J. 2001, Astrophys. J., 555, 448
Hagenaar, H. J., Schrijver, C. J., & Title, A. M. 2003, Astrophys. J., 584, 1107
Hagino, M., & Sakurai, T. 2004, PASJ, 56, 831
Hale, G. E. 1908, Astrophys. J., 28, 315
Hale, G. E., Ellerman, F., Nicholson, S. B., & Joy, A. H. 1919, Astrophys. J., 49, 153
Hale, G. E., & Nicholson, S. B. 1925, Astrophys. J., 62, 270
Hanasoge, S. M., Duvall, T. L., & Sreenivasan, K. R. 2012, Proceedings of the National Academy of Science, 109, 11928
Harvey, J. W., Branston, D., Henney, C. J., & Keller, C. U. 2007, Astrophys. J. Lett., 659, L177
Harvey, K. L. 1993, PhD thesis, , Univ. Utrecht, (1993)
Harvey, K. L., & Zwaan, C. 1993, Solar Phys., 148, 85
Hathaway, D. H. 1982, Solar Phys., 77, 341
Hathaway, D. H., Upton, L., & Colegrove, O. 2013, Science, 342, 1217
Hazra, G., Karak, B. B., & Choudhuri, A. R. 2014, Astrophys. J., 782, 93
Hotta, H., Rempel, M., & Yokoyama, T. 2012, Astrophys. J. Lett., 759, L24
—. 2015, Astrophys. J., 803, 42
—. 2016, Science, 351, 1427
Howard, R., & Labonte, B. J. 1980, Astrophys. J. Lett., 239, L33
Howe, R. 2009, Living Reviews in Solar Physics, 6
Iida, Y., Hagenaar, H. J., & Yokoyama, T. 2012, Astrophys. J., 752, 149
Ishikawa, R., & Tsuneta, S. 2009, Astron. Astrophys., 495, 607
Ishikawa, R., Tsuneta, S., Ichimoto, K., Isobe, H., Katsukawa, Y., Lites, B. W., Nagata, S., Shimizu, T., Shine, R. A., Suematsu, Y., Tarbell, T. D., & Title, A. M. 2008, Astron. Astrophys., 481, L25
Jabbari, S., Brandenburg, A., Kleeorin, N., Mitra, D., & Rogachevskii, I. 2015, Astrophys. J., 805, 166
Jackiewicz, J., Serebryanskiy, A., & Kholikov, S. 2015, Astrophys. J., 805, 133
Jiang, J., Cameron, R. H., Schmitt, D., & Schüssler, M. 2011, Astron. Astrophys., 528, A83
Jouve, L., & Brun, A. S. 2009, Astrophys. J., 701, 1300

Jouve, L., Brun, A. S., & Aulanier, G. 2013, Astrophys. J., 762, 4
Kazachenko, M. D., Fisher, G. H., & Welsch, B. T. 2014, Astrophys. J., 795, 17
Kazachenko, M. D., Fisher, G. H., Welsch, B. T., Liu, Y., & Sun, X. 2015, Astrophys. J., 811, 16
Khomenko, E. V., Collados, M., Solanki, S. K., Lagg, A., & Trujillo Bueno, J. 2003, Astron. Astrophys., 408, 1115
Kiepenheuer, K. O. 1968, in IAU Symposium, Vol. 35, Structure and Development of Solar Active Regions, ed. K. O. Kiepenheuer, 3
Komm, R., González Hernández, I., Hill, F., Bogart, R., Rabello-Soares, M. C., & Haber, D. 2013, Solar Phys., 287, 85
Krause, F., & Rädler, K. 1980, Mean-field magnetohydrodynamics and dynamo theory (Pergamon Press)
Kuckein, C., Martínez Pillet, V., & Centeno, R. 2012, Astron. Astrophys., 539, A131
Langfellner, J., Gizon, L., & Birch, A. C. 2015, Astron. Astrophys., 581, A67
Leka, K. D. 1999, Solar Phys., 188, 21
Leka, K. D., Canfield, R. C., McClymont, A. N., & van Driel-Gesztelyi, L. 1996, Astrophys. J., 462, 547
Leka, K. D., & Skumanich, A. 1999, Solar Phys., 188, 3
Li, Y., & Welsch, B. T. 2008, in Astronomical Society of the Pacific Conference Series, Vol. 383, Subsurface and Atmospheric Influences on Solar Activity, ed. R. Howe, R. W. Komm, K. S. Balasubramaniam, & G. J. D. Petrie, 397
Lites, B. W. 2009, Space Sci. Rev., 144, 197
Lites, B. W., Kubo, M., Socas-Navarro, H., Berger, T., Frank, Z., Shine, R., Tarbell, T., Title, A., Ichimoto, K., Katsukawa, Y., Tsuneta, S., Suematsu, Y., Shimizu, T., & Nagata, S. 2008, Astrophys. J., 672, 1237
Lites, B. W., Leka, K. D., Skumanich, A., Martinez Pillet, V., & Shimizu, T. 1996, Astrophys. J., 460, 1019
Lites, B. W., Skumanich, A., & Martinez Pillet, V. 1998, Astron. Astrophys., 333, 1053
Lockwood, M., Rouillard, A. P., & Finch, I. D. 2009, Astrophys. J., 700, 937
Longcope, D. W., & Fisher, G. H. 1996, Astrophys. J., 458, 380
Longcope, D. W., Fisher, G. H., & Pevtsov, A. A. 1998, Astrophys. J., 507, 417
Longcope, D. W., & Klapper, I. 1997, Astrophys. J., 488, 443
Longcope, D. W., & Welsch, B. T. 2000, Astrophys. J., 545, 1089
MacGregor, K. B., & Charbonneau, P. 1999, Astrophys. J., 519, 911
Mackay, D., & Yeates, A. 2012, Living Reviews in Solar Physics, 9
Mackay, D. H. 2015, in Astrophysics and Space Science Library, Vol. 415, Solar Prominences, ed. J.-C. Vial & O. Engvold, 355
Mackay, D. H., DeVore, C. R., & Antiochos, S. K. 2014, Astrophys. J., 784, 164
MacTaggart, D., & Hood, A. W. 2010, Astrophys. J. Lett., 716, L219
Martin, S. F., Livi, S. H. B., & Wang, J. 1985, Australian Journal of Physics, 38, 929
Martínez González, M. J., & Bellot Rubio, L. R. 2009, Astrophys. J., 700, 1391
Martínez Pillet, V. 2013, Space Science Reviews, 178, 141
Meyer, F., Schmidt, H. U., & Weiss, N. O. 1977, MNRAS, 179, 741
Meyer, K. A., Mackay, D. H., van Ballegooijen, A. A., & Parnell, C. E. 2011, Solar Phys., 272, 29
Miesch, M. S., & Dikpati, M. 2014, Astrophys. J. Lett., 785, L8
Moffatt, H. K. 1969, J. Fluid Mech., 35, 117
Moffatt, H. K. 1978, Magnetic field generation in electrically conducting fluids
Moffatt, H. K., & Ricca, R. L. 1992in , Royal Society of London, 411–429
Moreno-Insertis, F., Caligari, P., & Schüessler, M. 1994, Solar Phys., 153, 449
Moreno-Insertis, F., Caligari, P., & Schüssler, M. 1995, Astrophys. J., 452, 894
Nelson, N. J., Brown, B. P., Brun, A. S., Miesch, M. S., & Toomre, J. 2011, Astrophys. J. Lett., 739, L38
—. 2013, Astrophys. J., 762, 73
Nelson, N. J., Brown, B. P., Sacha Brun, A., Miesch, M. S., & Toomre, J. 2014, Solar Phys., 289, 441
Ortiz, A., Bellot Rubio, L. R., Hansteen, V. H., de la Cruz Rodríguez, J., & Rouppe van der Voort, L. 2014, Astrophys. J., 781, 126

Ossendrijver, M., Stix, M., & Brandenburg, A. 2001, Astron. Astrophys., 376, 713
Pariat, E., Aulanier, G., Schmieder, B., Georgoulis, M. K., Rust, D. M., & Bernasconi, P. N. 2004, Astrophys. J., 614, 1099
Parker, E. N. 1955, Astrophys. J., 121, 491
Parnell, C. E. 2001, Solar Phys., 200, 23
Pevtsov, A. A., Berger, M. A., Nindos, A., Norton, A. A., & van Driel-Gesztelyi, L. 2014, Space Science Reviews, 186, 285
Pevtsov, A. A., Canfield, R. C., & Metcalf, T. R. 1994, Astrophys. J. Lett., 425, L117
Pevtsov, A. A., Canfield, R. C., & Metcalf, T. R. 1995, Astrophys. J. Lett., 440, L109
Pietarila Graham, J., Danilovic, S., & Schüssler, M. 2009, Astrophys. J., 693, 1728
Pinto, R. F., & Brun, A. S. 2013, Astrophys. J., 772, 55
Rädler, K.-H. 1980, Astron. Nachr., 301, 101
Rajaguru, S. P., & Antia, H. M. 2015, Astrophys. J., 813, 114
Rempel, M. 2007, Astrophys. J., 655, 651
—. 2014, Astrophys. J., 789, 132
Rempel, M. 2015, The Astrophysical Journal, 814, 125
Rempel, M., & Cheung, M. C. M. 2014, Astrophys. J., 785, 90
Rempel, M., & Schüssler, M. 2001, Astrophys. J. Lett., 552, L171
Rempel, M. D. 2001, Struktur und Ursprung starker Magnetfelder am Boden der solaren Konvektionszone (Niedersächsische Staats-und Universitätsbibliothek)
Riley, P., Linker, J. A., Mikić, Z., Lionello, R., Ledvina, S. A., & Luhmann, J. G. 2006, Astrophys. J., 653, 1510
Rüdiger, G., Brandenburg, A., & Pipin, V. V. 1999, Astronomische Nachrichten, 320, 135
Schad, A., Timmer, J., & Roth, M. 2013, Astrophys. J. Lett., 778, L38
Schlichenmaier, R., Bello González, N., Rezaei, R., & Waldmann, T. A. 2010, Astron. Nachr., 331, 563
Schmieder, B., Archontis, V., & Pariat, E. 2014, Space Science Reviews, 186, 227
Schmieder, B., Demoulin, P., Aulanier, G., & Golub, L. 1996, Astrophys. J., 467, 881
Schou, J., Antia, H. M., Basu, S., Bogart, R. S., Bush, R. I., Chitre, S. M., Christensen-Dalsgaard, J., Di Mauro, M. P., Dziembowski, W. A., Eff-Darwich, A., Gough, D. O., Haber, D. A., Hoeksema, J. T., Howe, R., Korzennik, S. G., Kosovichev, A. G., Larsen, R. M., Pijpers, F. P., Scherrer, P. H., Sekii, T., Tarbell, T. D., Title, A. M., Thompson, M. J., & Toomre, J. 1998, Astrophys. J., 505, 390
Schrijver, C. J., & De Rosa, M. L. 2003, Solar Phys., 212, 165
Schrijver, C. J., & Harvey, K. L. 1994, Solar Phys., 150, 1
Schrijver, C. J., Title, A. M., van Ballegooijen, A. A., Hagenaar, H. J., & Shine, R. A. 1997, Astrophys. J., 487, 424
Schüssler, M. 1981, Astron. Astrophys., 94, L17
Schüssler, M., Caligari, P., Ferriz-Mas, A., & Moreno-Insertis, F. 1994, Astron. Astrophys., 281, L69
Schüssler, M., Caligari, P., Ferriz-Mas, A., Solanki, S. K., & Stix, M. 1996, Astron. Astrophys., 314, 503
Schüssler, M., & Vögler, A. 2008, Astron. Astrophys., 481, L5
Seehafer, N. 1990, Solar Phys., 125, 219
—. 1996, Physical Review E, 53, 1283
Simon, G. W., Title, A. M., & Weiss, N. O. 2001, Astrophys. J., 561, 427
Spruit, H. C. 1981, Astron. Astrophys., 98, 155
Spruit, H. C. 2003, Solar Phys., 213, 1
Spruit, H. C., & van Ballegooijen, A. A. 1982, Astron. Astrophys., 106, 58
Stein, R. F., & Nordlund, Å. 2012, Astrophys. J. Lett., 753, L13
Sterling, A. C., Chifor, C., Mason, H. E., Moore, R. L., & Young, P. R. 2010, Astron. Astrophys., 521, A49
Stix, M. 1976, Astron. Astrophys., 47, 243
Strous, L. H., & Zwaan, C. 1999, Astrophys. J., 527, 435
Thaler, I., & Spruit, H. C. 2015, Astron. Astrophys., 578, A54
Thompson, M. J., Christensen-Dalsgaard, J., Miesch, M. S., & Toomre, J. 2003, ARA&A, 41, 599

Thompson, M. J., Toomre, J., Anderson, E. R., Antia, H. M., Berthomieu, G., Burtonclay, D., Chitre, S. M., Christensen-Dalsgaard, J., Corbard, T., De Rosa, M., Genovese, C. R., Gough, D. O., Haber, D. A., Harvey, J. W., Hill, F., Howe, R., Korzennik, S. G., Kosovichev, A. G., Leibacher, J. W., Pijpers, F. P., Provost, J., Rhodes, Jr., E. J., Schou, J., Sekii, T., Stark, P. B., & Wilson, P. R. 1996, Science, 272, 1300
Tian, L., Bao, S., Zhang, H., & Wang, H. 2001, Astron. Astrophys., 374, 294
Tobias, S. M., Cattaneo, F., & Boldyrev, S. 2013, in Ten Chapters in Turbulence (Cambridge University Press)
Tomczyk, S., Schou, J., & Thompson, M. J. 1995, Astrophys. J. Lett., 448, L57
Toriumi, S., Iida, Y., Kusano, K., Bamba, Y., & Imada, S. 2014, Solar Phys., 289, 3351
Trujillo Bueno, J., Shchukina, N., & Asensio Ramos, A. 2004, Nature, 430, 326
van Ballegooijen, A. A. 1982, Astron. Astrophys., 113, 99
van Ballegooijen, A. A., & Mackay, D. H. 2007, Astrophys. J., 659, 1713
van Ballegooijen, A. A., & Martens, P. C. H. 1989, Astrophys. J., 343, 971
van Driel-Gesztelyi, L., Démoulin, P., Mandrini, C. H., Harra, L., & Klimchuk, J. A. 2003, Astrophys. J., 586, 579
van Driel-Gesztelyi, L., & Green, L. M. 2015, Living Rev. Solar Phys., 8
van Driel-Gesztelyi, L., Malherbe, J.-M., & Démoulin, P. 2000, Astron. Astrophys., 364, 845
Vögler, A., & Schüssler, M. 2007, Astron. Astrophys., 465, L43
Wang, J., & Shi, Z. 1993, Solar Phys., 143, 119
Wang, Y.-M. 2013, Astrophys. J. Lett., 775, L46
Wang, Y.-M., Lean, J., & Sheeley, Jr., N. R. 2000, Geophys. Res. Lett., 27, 505
Wang, Y.-M., Nash, A. G., & Sheeley, Jr., N. R. 1989, Science, 245, 712
Webb, D. F., & Howard, T. A. 2012, Living Rev. Solar Phys., 9
Weber, M. A., Fan, Y., & Miesch, M. S. 2011, Astrophys. J., 741, 11
Weber, M. A., Fan, Y., & Miesch, M. S. 2013, Solar Phys., 287, 239
Woltjer, L. 1958, Proc. Natl. Acad. Sci. USA, 44, 489
Yang, W. H., Sturrock, P. A., & Antiochos, S. K. 1986, Astrophys. J., 309, 383
Yardley, S. L., Green, L. M., Williams, D. R., van Driel-Gesztelyi, L., & Dacie, S. 2016, Astrophys. J., submitted
Yeates, A. R., & Muñoz-Jaramillo, A. 2013, 436, 3366
Zhao, J., Bogart, R. S., Kosovichev, A. G., Duvall, Jr., T. L., & Hartlep, T. 2013, Astrophys. J. Lett., 774, L29
Zwaan, C. 1978, Solar Phys., 60, 213
—. 1985, Solar Phys., 100, 397